THE UNIVERSITY of EDINBURGH

Edinburgh Research Explorer

# Importance of second-order wave generation for focused wave group run-up and overtopping.

**Citation for published version:**
Orszaghova, J, Taylor, P, Borthwick, A & Raby, A 2014, 'Importance of second-order wave generation for focused wave group run-up and overtopping.', *Coastal Engineering*, vol. 94, pp. 63-79. https://doi.org/10.1016/j.coastaleng.2014.08.007

**Digital Object Identifier (DOI):**
10.1016/j.coastaleng.2014.08.007

**Link:**
Link to publication record in Edinburgh Research Explorer

**Document Version:**
Early version, also known as pre-print

**Published In:**
Coastal Engineering

**General rights**
Copyright for the publications made accessible via the Edinburgh Research Explorer is retained by the author(s) and / or other copyright owners and it is a condition of accessing these publications that users recognise and abide by the legal requirements associated with these rights.

**Take down policy**
The University of Edinburgh has made every reasonable effort to ensure that Edinburgh Research Explorer content complies with UK legislation. If you believe that the public display of this file breaches copyright please contact openaccess@ed.ac.uk providing details, and we will remove access to the work immediately and investigate your claim.

OPEN ACCESS

Download date: 12. Oct. 2024

*Manuscript
Click here to view linked References

# Importance of second-order wave generation for focused wave group run-up and overtopping

Jana Orszaghova[a,*], Paul H. Taylor[b,*], Alistair G.L. Borthwick[c,*], Alison C. Raby[d,*]

[a] *HR Wallingford, Howbery Park, Wallingford, Oxfordshire, OX10 8BA, UK*
[b] *Department of Engineering Science, University of Oxford, Parks Road, Oxford, OX1 3PJ, UK*
[c] *School of Engineering, The University of Edinburgh, The King's Buildings, Edinburgh EH9 3JL, UK*
[d] *School of Marine Science and Engineering, University of Plymouth, Drake Circus, Plymouth, PL4 8AA, UK*

## Abstract

Focused wave groups offer a means for coastal engineers to determine extreme run-up and overtopping events. Numerical predictions and laboratory measurements are presented for NewWave-type focused wave groups generated by a piston-type paddle generator, and interacting with a plane beach and a seawall in a wave basin. The numerical wave tank is based on the Boussinesq equations for non-breaking waves, and the non-linear shallow water equations for broken waves. Good agreement is achieved between the numerical predictions and laboratory measurements of free surface elevation, run-up distances and overtopping volumes for the test cases driven by linear paddle signals. Errors in run-up distance and overtopping volume are then assessed by repeating the test cases using second-order accurate wave generation signals. Focused wave groups generated using first-order wave-maker theory are found to be substantially contaminated by a preceding long error wave, resulting in erroneously enhanced run-up distances and overtopping volumes. Thus, the use of second-order wave-maker theory for wave group run-up and overtopping experiments is instead recommended.

*Keywords:* wave-maker theory, spurious error wave, run-up, overtopping, focused wave groups, numerical wave tank, Boussinesq modelling

## 1. Introduction

Accurate prediction of coastal wave run-up and overtopping is very important in scenario-driven analysis of likely flood events (see e.g. Kobayashi (1999), Borthwick (2009), Baldock et al. (2012)). Considerable effort has been put into deriving empirical run-up and overtopping formulae (see e.g. Hunt (1959), Hedges and Mase (2004), Hedges and Reis (2004), Allsop et al. (2005), De Rouck et al. (2005), Burcharth and Hughes (2006), Pullen et al. (2007)), supplemented by a great number of wave tests in different flumes and coastal basins

*j.orszaghova@hrwallingford.com, +44 (0)1491 822309

(see e.g. Pearson et al. (2002), van der Meer et al. (2009) and Hunt-Raby et al. (2011)). There have also been major developments in coastal wave simulation methods, some based on the non-linear shallow water equations (e.g. Hu et al. (2000), Hubbard and Dodd (2002)), Boussinesq-type equations (see for example Fuhrman and Madsen (2008) or review documents by Dingemans (1997), Kirby (1997), Madsen and Schäffer (1999), Kirby (2003), Brocchini (2013)), hybrid Boussinesq-shallow flow equations (Watson et al. (1994), Borthwick et al. (2006a), Tonelli and Petti (2009), Tissier et al. (2011), Orszaghova et al. (2012), McCabe et al. (2013)), potential flow theory (Fructus and Grue (2007)), and the Navier-Stokes equations (see e.g. Hsiao and Lin (2010) for volume-of-fluid method, Ingram et al. (2009) for free surface tracking implementation, and Rogers and Dalrymple (2008) for a smoothed particle hydrodynamics solver).

For almost 20 years, focused wave groups have been increasingly used by offshore engineers to represent the average shape of the extreme event in a Gaussian sea state (Tromans et al. (1991), Jonathan and Taylor (1997), Taylor and Williams (2004)). Pioneering laboratory experiments on focused wave groups have been carried out in water of uniform depth (Rapp and Melville (1990), Baldock et al. (1996) and Johannessen and Swan (2001)), demonstrating that ocean waves are dispersive and can evolve into transient, localised but energetic groups that focus in shallow coastal waters (Baldock (2006)). It is also plausible that similar focused-wave analysis could be useful in assessing storm-induced wave run-up maxima at beaches and overtopping volumes at coastal defences. Focused wave group laboratory tests have the advantage that they are quick to perform, with all important data obtained before any waves reflected at the coast reach the paddle, thus avoiding the gradual contamination of flumes by long wave reflections. However, it should be noted that there remain several important questions to be answered regarding the applicability of focused wave groups as design waves for extreme storm events at the coast. In reality, wave run-up at beaches and sea defence overtopping are strongly influenced by the preceding swash motions, and it is not necessarily the case that the peak run-up or overtopping is associated with the largest wave. Moreover, the near-shore wave energy spectrum is not the same as the corresponding offshore spectrum. Even so, there is a sound rationale for investigating systematically the behaviour of focused wave groups in coastal waters.

The present paper examines a preliminary question concerning the order of accuracy required for the paddle signal used to generate focused waves in a basin or flume. In particular, we examine the importance of the correct reproduction of second-order bound components in focused wave groups, and study their influence on wave group run-up at a plane beach and overtopping of a seawall. To this end, results are compared from laboratory and numerical tests, the latter utilising linear and second-order wave generation methods. The numerical wave flume is based on the Madsen and Sørensen (1992) set of Boussinesq equations and the non-linear shallow water equations. As direct comparisons with laboratory experiments are carried out, waves are introduced into the numerical domain via an in-built moving piston wave-maker, which mimics a mechanical laboratory wave generator. Details of the numerical scheme are given in Orszaghova et al. (2012).

The paper is structured as follows. Section 2 provides an introduction to wave-maker theory, NewWave focused wave groups, and the numerical wave tank. Section 3 describes a

numerical model investigation into focused wave group evolution over a flat bed, using linear and second-order wave generation. Major discrepancies are identified in the resulting wave forms, these arising from error waves when only first-order wave generation is used. The numerical model is validated against experimental measurements involving wave group run-up at a plane beach (Section 4) and overtopping of a trapezoidal wall (Section 5). In both sections, the effect of second-order wave generation on focused wave run-up distances and overtopping volumes is examined numerically. Section 6 summarises the major conclusions.

## 2. Methods and background theory

### *2.1. Laboratory wave generation*

Piston paddles are often used for mechanical wave generation in shallow water laboratory flumes and basins. In practice, a suitable wave-maker theory is used to compute the paddle displacement time series used to control the horizontal motion of the paddle. The wave-maker theory for irregular waves utilises a Stokes-like perturbation technique, whereby the dependent variables (velocity potential $\Phi$, free surface elevation $\zeta$, paddle displacement $x_p$) are expressed as a power series, and the boundary conditions at the free surface and at the wave-maker are expanded using Taylor series. This results in the original non-linear boundary value problem being expressed as an infinite set of ordered linear partial differential equations. First-order wave-maker theory considers the linearised problem, whose solution consists of the desired progressive harmonic waves and evanescent modes. Evanescent modes are local non-propagating disturbances that arise due to a uniform velocity field with depth being forced at the piston paddle, but die out away from the wave-maker. The relationship between the amplitude of the generated progressive wave and the amplitude of the paddle displacement is also derived, and is known as the Biésel paddle transfer function. Detailed descriptions of linear wave-maker theory are given by Dean and Dalrymple (1991) and Hughes (1993).

Full wave generation theory correct to second order, for normally propagating waves and applicable to both piston and hinged wave-makers, was derived by Schäffer (1996), who extended earlier analysis by Barthel et al. (1983). Schäffer's theory aims to suppress generation of second-order spurious free waves, also known as parasitic or error waves, which are unintentionally generated when linear paddle signals are used. A brief outline of Schäffer's theory follows. Using the superposition principle, the second-order problem is split into three sub-problems, each governed by the Laplace equation and a specific set of boundary conditions. The first sub-problem considers the wave in the absence of the wave-maker, and is solved to give the bound second-order sub- and super-harmonics. The other two sub-problems bear resemblance to the first-order problem, and give rise to second-order free waves. The second sub-problem solves to give second-order error waves owing to the linear paddle signal deviating from the mean paddle position, and second-order bound waves not satisfying the paddle boundary condition. The third sub-problem describes the compensating second-order free waves generated by the second-order paddle signal, which is chosen to cancel out the error waves from the second sub-problem. In this way only the appropriate

bound second-order waves are generated. Note, however, that the evanescent modes from the second and third sub-problems do not cancel each other out.

Simplistically, the use of linear wave generation results in the following situation. The desired weakly non-linear waves have both linear energy-bearing components and higher, mostly second-order, bound components. If these higher harmonics are not accounted for by the paddle motion, the resulting wave field consists of the correct bound non-linear components and locally cancelling sum and difference components. These are free error waves but locally (at the paddle) cancel the necessary bound components. Since these free waves have different propagation speeds than the main linear waves in the desired wave group, they escape and contaminate the overall wave field.

### *2.2. Numerical wave tank*

A one-dimensional numerical model of a shallow-water flume with an in-built piston paddle moving boundary wave-maker is used for all simulations in this work. The model is based on a set of enhanced Boussinesq equations derived by Madsen and Sørensen (1992) and the non-linear shallow water equations. Wave breaking is described approximately, by locally switching to the non-linear shallow water equations when specified threshold wave steepness is reached. Broken waves are described as bores. The moving shoreline is calculated as part of the solution, utilising a wetting and drying approach devised by Brufau et al. (2002). Detailed description of the model's characteristics, including numerical implementation, is given by Orszaghova et al. (2012). The model is suitable for simulating propagation of weakly dispersive waves and can additionally model any associated inundation, overtopping or inland flooding within the same simulation. Note that the in-built piston paddle wave-maker mimics a real-world laboratory wave-maker in that it moves according to a supplied paddle displacement time series calculated using appropriate wave-maker theory (see Section 2.1 above). The paddle operates on a local movable grid, which is Lagrangian on the paddle face and Eulerian away from the paddle. The governing equations are, however, evolved on a fixed mapped grid, and the newly calculated solution is transformed back onto the moving grid via a domain mapping technique. Inclusion of the paddle in the numerical code allows for simulations of complete shallow water laboratory experiments, including the wave generation process, by utilising the actual paddle displacement time series used in the laboratory.

Orszaghova et al. (2012) provide a detailed account of tests used to verify the numerical model, encompassing movement of the wet/dry front, wave generation by means of the numerical paddle, and discretisation of the governing equations. Orszaghova et al. (2012) also report preliminary validation of the code against a range of laboratory experiments. The present paper provides additional validation of the numerical model, before embarking on the assessment of the use of linear paddle signals in run-up and overtopping studies involving wave groups.

It should be noted that the chosen set of Boussinesq equations used in the numerical wave tank is suitable for weakly dispersive and weakly non-linear waves. Numerous improved versions of Boussinesq-type equations have also been derived extending their validity both offshore and inshore (see e.g. Wei et al. (1995), Agnon et al. (1999), Gobbi et al. (2000),

Madsen et al. (2003)). The validation tests, described later, show that the Madsen and Sørensen (1992) Boussinesq equations are sufficient to assess the importance of second-order wave generation for the focused wave groups considered herein.

### *2.3. NewWave focused wave groups*

A focused wave group is composed of a number of individual sinusoidal wave components that come into phase at a single point in time and space. The surface elevation, using linear wave theory, at any time and any point in space can be described by

$$\zeta(x,t) = \sum_{n=1}^{N} a_n \cos(k_n(x - x_f) - \omega_n(t - t_f) + \phi), \tag{1}$$

where $x$ is horizontal distance, $t$ is time, $a_n$ is the wave amplitude, $k_n$ is the wave number, and $\omega_n$ is the angular frequency of the $n^{\text{th}}$ component, $\phi$ is the phase angle at focus, $x_f$ and $t_f$ are the focus location and focus time, and $N$ is the number of the Fourier components. At $x = x_f$ and $t = t_f$ all wave components are in-phase. A crest-focused wave group is given by $\phi = 0$, whereby wave crests come into phase at the focus point. A trough-focused wave group, with wave troughs aligning at the focus location, is defined by $\phi = \pi$. Note in passing that this is equivalent to replacing $a_n$ by $-a_n$ in Equation (1), which shall be utilised in the separation of harmonics presented in Sections 3 - 5. When focused, constructive interference between individual components occurs and the wave group produces a large energetic event. Due to frequency dispersion, away from focus, the wave group is less compact and less violent. In the laboratory, to create a focused wave group with desired $x_f$ and $t_f$ one needs to offset correctly the individual wave components at the paddle to account for their different propagation speeds along the tank. Using Equation (1), a phase shift of $-k_n x_f + \phi$ is applied to each $n^{\text{th}}$ component, assuming that the wave-maker is located at $x = 0$ m and that $t_f = 0$ s.

NewWave focused wave group is consistent with the mathematical description of the expected shape of extreme wave events in a linear random sea, as shown by Jonathan and Taylor (1997) and Taylor and Williams (2004). The underlying statistical theory originates from Lindgren (1970) and Boccotti (1983), and was first applied to extreme wave events in ocean engineering by Tromans et al. (1991). According to the theory (see e.g. Tucker and Pitt (2001)), the most probable shape of the free surface near an arbitrary crest is given by the normalised autocorrelation function pre-multiplied by the crest height. The NewWave time history, for a crest-focused wave, therefore reads as

$$\zeta(t) = A_{\mathcal{N}} \frac{\sum_n S_n(\omega)\Delta\omega_n \cos(\omega_n(t - t_f))}{\sum_n S_n(\omega)\Delta\omega_n}, \tag{2}$$

where $A_{\mathcal{N}}$ is the linear amplitude of the NewWave group at focus, $S_n$ is the discretised underlying energy spectrum from which the extreme wave packet is derived and $\Delta\omega_n$ is the

angular frequency resolution. In Equation (2) the numerator represents the autocorrelation function, given by the inverse Fourier transform of the underlying spectrum, and the denominator represents the normalising factor. In the NewWave representation, the individual wave amplitudes $a_n$ are thus given by

$$a_n = \frac{A_{\mathcal{N}} S_n(\omega)\Delta\omega_n}{\sum_n S_n(\omega)\Delta\omega_n}. \tag{3}$$

Note that the choice of $A_{\mathcal{N}}$ is arbitrary as it represents the amplitude of the largest wave in a sea surface time series of $\mathcal{N}$ waves in a narrow-banded linear random sea. In other words, the return period of a wave packet with amplitude $A_{\mathcal{N}}$ is 1 in $\mathcal{N}$ waves within the sea state. Therefore, assuming Rayleigh wave height distribution, $A_{\mathcal{N}}$ is given by

$$A_{\mathcal{N}} = \left(2\sigma^2 \ln \mathcal{N}\right)^{1/2}, \tag{4}$$

where $\sigma^2$ denotes the variance of the free surface time series. Laboratory experiments and numerical simulations involving NewWaves benefit from the complete spectral information contained in the single wave group, and so investigations are relatively quick and inexpensive compared to their random wave time domain counterparts. Additionally, due to their transient nature, active wave absorption at the wave-maker is not required for focused wave investigations.

### *2.4. UKCRF experiments*

The experimental measurements used to validate the present model were obtained from laboratory-scale tests undertaken at the U.K. Coastal Research Facility (UKCRF) at HR Wallingford comprising a 72 paddle wave basin with a plane beach of bed slope 1:20. The mean water depth at the paddles was set to 0.5 m, with horizontal bed extending 8.33 m from the paddles to the toe of the plane beach. The experimental measurements were undertaken as part of an EPSRC-funded investigation undertaken jointly by the Universities of Manchester and Oxford in 2001/2002 into the run-up and overtopping of focused wave groups. Details of the experiments are reported by Hunt (2003), Borthwick et al. (2006b) and Hunt-Raby et al. (2011). As part of the experimental programme, a total of eight normally-incident NewWave focused wave groups were considered, involving four crest-focused and four trough-focused wave groups, covering a range of group amplitudes and focus locations. Table 1 summarises the wave group properties. There is a shift in the observed focus location away from the input focus location predicted by linear theory. Note that in the experiments, the focus location was defined as the point in space where the troughs either side of the central crest, for a crest-focused wave group, are of equal depth. The underlying energy spectrum used in the experiments was a Pierson-Moskowitz spectrum given by

$$S(\omega) = \left(\frac{\omega_p}{\omega}\right)^5 \exp\left(-1.25\left(\frac{\omega_p}{\omega}\right)^4\right), \tag{5}$$

with peak angular frequency $\omega_p \approx 2.91$ rad s$^{-1}$. The truncated spectrum ($\omega_{min} \approx 2.07$ rad s$^{-1}$, $\omega_{max} \approx 6.06$ rad s$^{-1}$) was discretised into $N = 53$ components with a uniform angular frequency increment of $\Delta\omega \approx 0.077$ rad s$^{-1}$. In the UKCRF laboratory experiments the paddle motion was governed by linear wave-maker theory, and active wave absorption was not applied.

Table 1: Properties of normally-incident NewWave focused wave groups in UKCRF (Hunt (2003)).

| Wave group | Input amplitude $A_{\mathcal{N}}$ (m) | Input focus location $x_f$ (m) | Observed focus location (m) | Phase angle at focus $\phi$ (rad) |
|---|---|---|---|---|
| WG1 | 0.114 | 9.00 | 8.33 | 0 |
| WG2 | 0.114 | 10.90 | 10.83 | 0 |
| WG3 | 0.090 | 12.90 | 13.33 | 0 |
| WG4 | 0.057 | 8.80 | 8.33 | 0 |
| WG5 | 0.114 | 9.00 | 8.33 | $\pi$ |
| WG6 | 0.114 | 10.90 | 10.83 | $\pi$ |
| WG7 | 0.090 | 12.90 | 13.33 | $\pi$ |
| WG8 | 0.057 | 8.80 | 8.33 | $\pi$ |

## 3. NewWave propagation on a flat bed

Before considering NewWave run-up and overtopping, we first investigate the effect of second-order error waves on the evolution over a flat bed of two focused wave groups, whose properties correspond to WG2 and WG6 (Table 1). Two simulations per wave group are carried out using the numerical wave tank; the first governed by the linear paddle signal recorded from the experiments, the second repeated using the corresponding second-order paddle signal calculated according to the method derived by Schäffer (1996). A symmetry-based method for separation of harmonics from the calculated free surface time series is used to identify the second-order error waves (for examples of the application of this method see e.g. Baldock et al. (1996), Jonathan and Taylor (1997), Johannessen and Swan (2001), Hunt et al. (2004) and Borthwick et al. (2006b)). The effectiveness of second-order paddle signals in eliminating the contaminating error waves is also examined.

Figure 1 shows first- and second-order paddle displacement time series, denoted by $x_p$, for the WG2 crest-focused and corresponding WG6 trough-focused wave groups. The second-order signal requires a much larger paddle sweep. Due to the finite number of frequency components ($N = 53$ for the present wave groups), the paddle signals have a finite repeat period given by $\frac{1}{\Delta f}$, with $\Delta f$ being the frequency increment. The repeat period for the present wave groups is 81.92 s.

It is useful to recall that the Schäffer (1996) second-order wave-maker theory is based on second-order solutions to the full Laplace equation water wave problem (together with the appropriate boundary conditions), rather than the Madsen and Sørensen (1992) Boussinesq equation set used herein. The Boussinesq equations are a weakly dispersive and weakly

non-linear approximation of the full water wave problem. Therefore for relatively low-amplitude waves in shallow water, the second-order paddle signals calculated according to Schäffer (1996) should satisfactorily eliminate the spurious second-order error waves in the Boussinesq numerical tank. Figure 2 shows the time series of the theoretically derived bound sub-harmonics and super-harmonics for the WG2 crest-focused wave group. The time series are calculated at the paddle ($x = 0$ m) in the absence of evanescent modes. Both the Laplace equation and the Boussinesq equations second-order bound solutions are shown. Note that the second-order bound components for the Boussinesq equations are calculated according to Madsen and Sørensen (1993). In order to suppress formation of second-order error waves, the bound harmonics need to be correctly accounted for at the paddle. From Figure 2 it follows that the Laplace super-harmonic components are larger than the Boussinesq super-harmonic components. Therefore, it might be expected that some small excess sum frequency waves will be generated and propagate as free waves when the calculated second-order signal is fed into the present model. On the other hand, the Laplace sub-harmonic components are marginally smaller than the Boussinesq long wave components, suggesting that the long error wave will be almost perfectly eliminated.

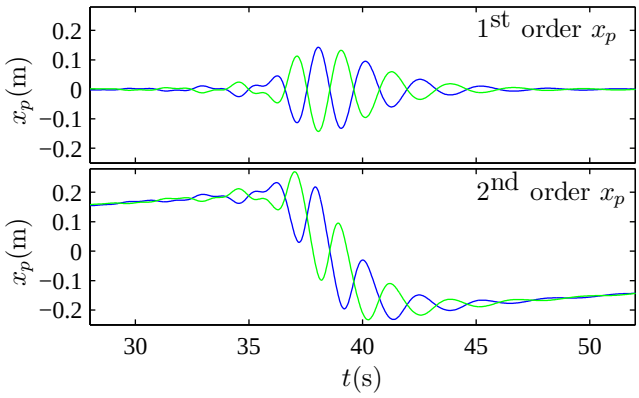


Figure 1: Paddle displacement time series for the WG2 crest-focused wave group (blue line) and the WG6 trough-focused wave group (green line). First-order paddle signals are shown in the top plot. Corresponding second-order paddle signals are shown in the bottom plot.

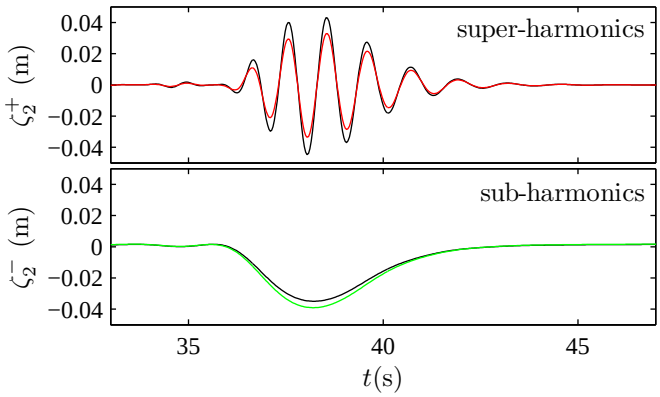


Figure 2: Second-order bound super-harmonic (top plot) and sub-harmonic (bottom plot) time series at $x = 0$ for the WG2 crest-focused wave group. Comparison between the second-order components for the Laplace equation (black line) and the Boussinesq equations (red line for super-harmonics, green line for sub-harmonics).

Figures 3, 5, 6 and 7 present a comparison between using first- (left plot) and second-order paddle signals (right plot) for wave groups WG2 and WG6 propagating over a flat bed. Each figure comprises an $x - t$ contour plot of stacked free surface time series calculated by the model. The free surface deviation from the still water level is expressed by the colour: whereby positive elevation is shown by yellow, orange and red; and depression is shown by different shades of blue. Note that the units of the colour scale are meters. It is emphasised that each plot shows an evolving wave group (in a flume), and does not represent a snapshot of a two-dimensional sea-state (in a basin).

Figure 3 presents the $x - t$ propagation plot for the WG2 crest-focused wave group. In both cases, the group is initially compact around the focus and spans roughly 7 s. As it propagates further away from the paddles, the group disperses, expanding over the remaining 20 s shown. However, there are stark visual differences between the results obtained using a first- and a second-order paddle signal. Remember that the two plots refer nominally to the same wave group. The left and central crests are higher in the first-order case for the entire propagation. On the other hand, the left trough is deeper in the second-order case throughout the record. Plots for WG6, the corresponding trough-focused group, are omitted for brevity.

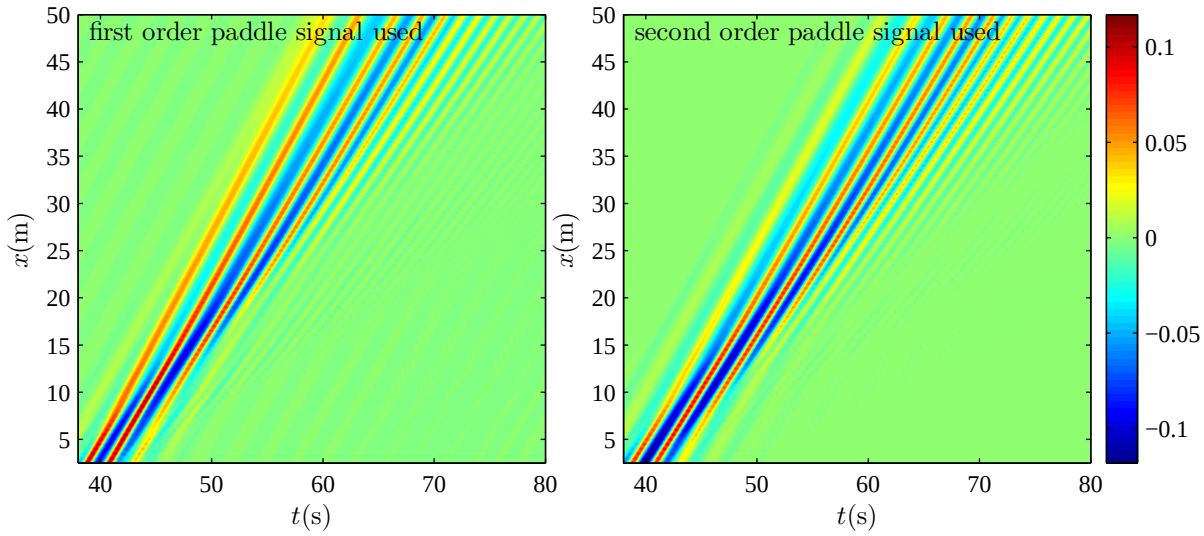


Figure 3: NewWave propagation on a flat bed - **total free surface** for the WG2 crest-focused wave group. Model predictions using a first-order paddle signal (left plot) and a second-order paddle signal (right plot).

An approximate separation of harmonics is performed in order to carry out a more detailed analysis of the structure of the wave packet. Let the free surface time series of the crest-focused wave be denoted by $\zeta_c$ and that of the trough-focused wave by $\zeta_t$. Recall that a crest-focused group and a corresponding trough-focused group are related via a phase shift of $\pi$ rad, which is of course equivalent to pre-multiplying each $a_n$ by -1 in Equation (1). Therefore, addition $\frac{1}{2}(\zeta_c + \zeta_t)$ gives the even-order harmonics as the linear components and other odd-order harmonics cancel out. Subtraction $\frac{1}{2}(\zeta_c - \zeta_t)$ results in the linear components and all the odd-order harmonics. Frequency filtering can be additionally used to extract the required harmonics from the addition and subtraction time series. Suitable cut-off frequencies for the applied high-pass and low-pass filters are obtained from the frequency spectra. Figure 4 displays the amplitude spectra associated with the crest-focused time series (top plot), the addition time series (middle plot) and the subtraction time series (bottom plot) from $x = 8.33$ m, which is the location of the beach toe in the run-up and overtopping studies later. Amplitude spectra are shown for the wave group generated with the first-order paddle signal (black line) and the second-order paddle signal (red line). From the figure, it follows that for the addition time series, which contains the even harmonics, a cut-off frequency of 0.5 Hz can be used to separate the sub-harmonics (denoted by $2^-$) from the super-harmonics (denoted by $2^+$). For the subtraction time series, which contains the odd harmonics, a cut-off frequency of 1 Hz is used to separate the linear terms (denoted by 1) from the third- (denoted by $3^+$) and higher-order odd harmonics. Amplitude spectra are obtained by applying a Fast Fourier Transform (FFT) algorithm to the time series. After frequency filtering is performed, the inverse transform recovers the filtered time series. It should be noted that this separation of harmonics is only approximate due to non-linear wave-wave interactions, whereby for example in the linear paddle signal case a sub-harmonic

interaction between the linear and the free second-order sum components generates third-order components in amplitude with frequencies lying within the primary frequencies band.

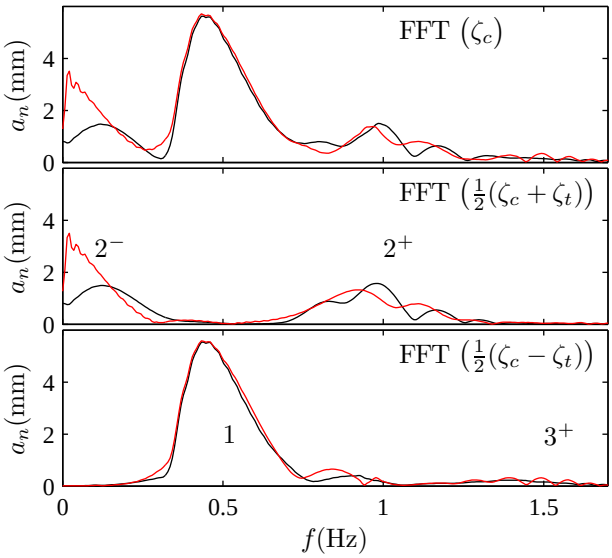


Figure 4: Amplitude spectra associated with the total free surface elevation time series (top plot), the addition time series (middle plot) and the subtraction time series (bottom plot) shown for the WG2 and WG6 pair of wave groups generated with the first-order paddle signal (black line) and the second-order paddle signal (red line).

Figure 5 shows the free surface subtraction time series, low-pass filtered at 1 Hz to isolate the linear terms. The two contour plots are rather similar, apart from small discrepancies at the left crest, confirming that the use of second-order paddle signals does not affect the primary frequency components.

Figure 6 shows the free surface addition time series, low-pass filtered at 0.5 Hz to isolate the difference frequency components. As can be seen from the two plots, the use of the second-order paddle signal substantially alters the structure of the long wave components. In the first-order plot, the long error wave manifests itself as a hump (positive elevation shown in orange and red). It is governed by its own dynamics and can be seen propagating ahead of the group due to its long wavelength. In the second-order plot, the long error wave is eliminated and the bound long waves can be clearly seen as a localised depression underneath the main wave group (shown in blue). These long wave plots help to explain observations from Figure 3, where higher left crests and shallower left troughs are identified in the first-order case. Note that a very faint yellow elevation can be seen ahead of the bound long wave in the second-order plot in Figure 6 (at $t > 50$ s), suggesting that the long error wave is not perfectly suppressed. This is most likely due to the second-order wave-maker theory from Schäffer (1996) being applied to the Boussinesq numerical solver. As noted earlier, the set-down for the Boussinesq equation is very slightly different to that of the non-linear potential flow equations. Nevertheless, the release of the long error wave is minimal.

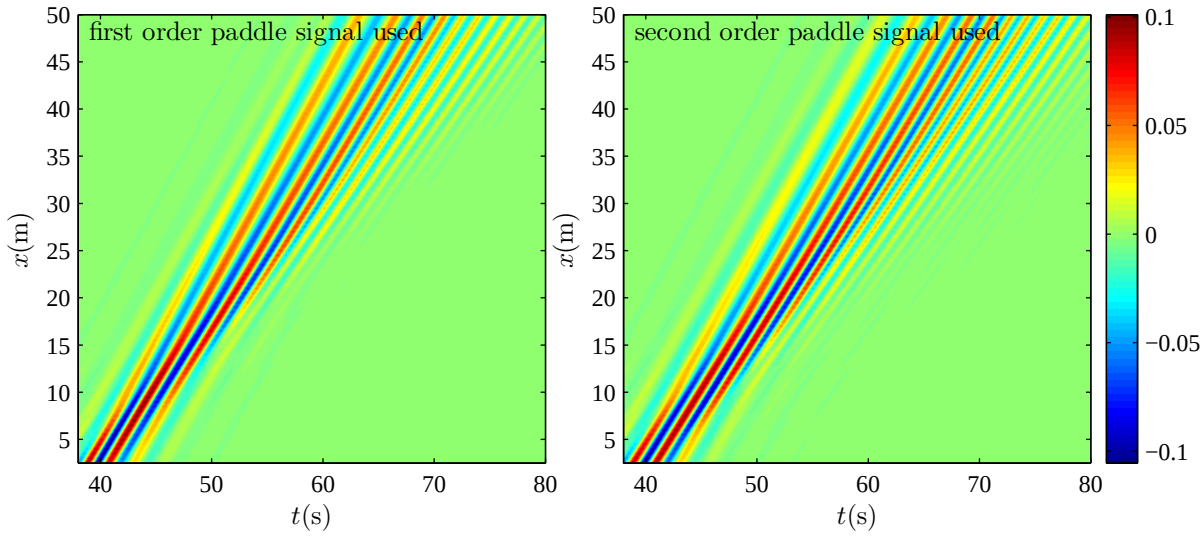


Figure 5: NewWave propagation on a flat bed - **linear terms** only. Model predictions using a first-order paddle signal (left plot) and a second-order paddle signal (right plot).

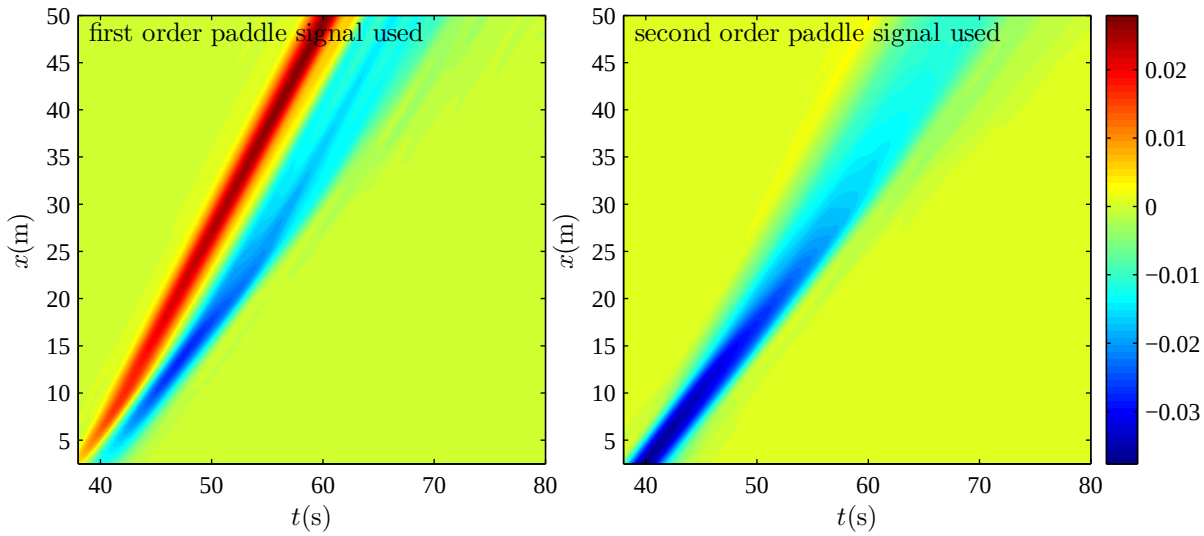


Figure 6: NewWave propagation on a flat bed - **long waves** only. Model predictions using a first-order paddle signal (left plot) and a second-order paddle signal (right plot).

Figure 7 shows the free surface addition time series, high-pass filtered at 0.5 Hz to extract the second-order sum components (and any other higher-order even harmonics). The bound second-order super-harmonics (denoted by b) can be seen in both plots, travelling with the speed of the main group, thus reaching $x = 50$ m at $t = 60 - 70$ s. The free error double frequency harmonics (denoted by e) can be seen lagging behind the main group. When using the second-order paddle signal, these error waves are weakened but not fully eliminated. As discussed earlier, this is probably due to the different second-order bound solution of the

Laplace equation and the Boussinesq equations. In Sections 4.2 and 5.2, the influence of second-order wave generation on run-up distances and overtopping volumes is investigated. Even though the sum frequency error waves are not fully eliminated, their presence will not spoil the investigation because they travel behind the main wave packet and arrive at the beach as a second distinctive packet after the main interaction is over.

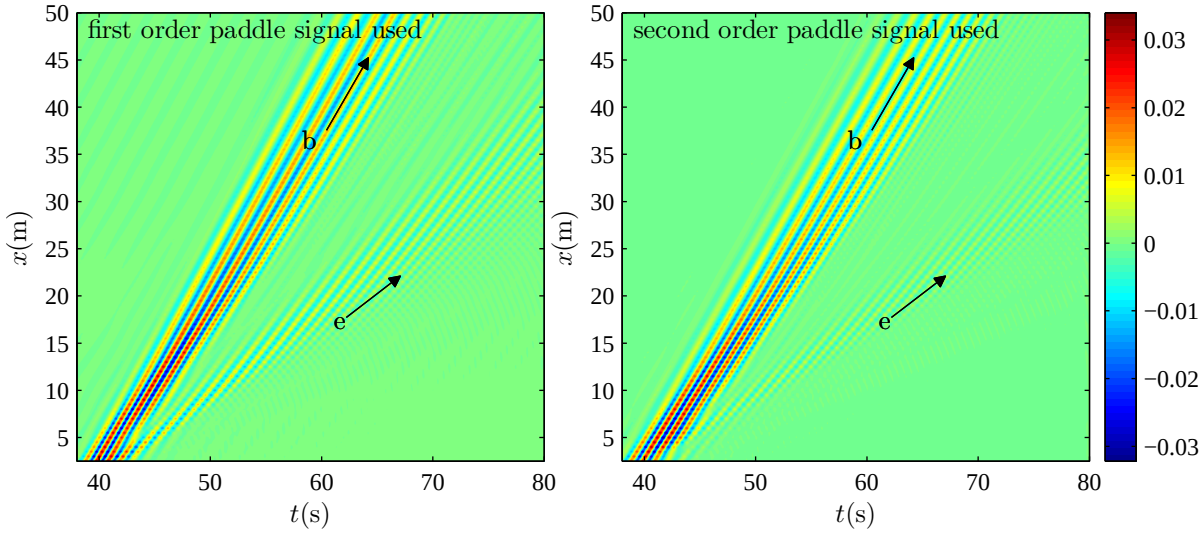


Figure 7: NewWave propagation on a flat bed - **even order super-harmonics** only. Model predictions using a first-order paddle signal (left plot) and a second-order paddle signal (right plot).

Figure 8 shows spatial profiles of the WG2 crest-focused wave group at three different times. The profiles generated by the first-order paddle signal are shown on the left, and the wave group generated by the second-order paddle signal is shown on the right. In the first-order plots, the long error wave (denoted by $2^-$) can be seen dramatically changing the front of the wave packet, increasing wave heights of the first few crests and flattening the leading troughs. Also in the first-order plots, the free second-order sum components can be seen following the main wave group (denoted by $2^+$). In the second-order plots, the weakened residual free second-order sum components can be seen (denoted by $2^+$). These are additionally followed by triple frequency free waves (denoted by $3^+$), which of course are not eliminated using second-order paddle signals.

In summary, the approximate method for separation of harmonics demonstrates that use of linear wave-maker theory leads to the release of a long error wave of substantial amplitude immediately ahead of the focus wave group. This error wave alters the local shape of the leading part of the transient wave group as it evolves.

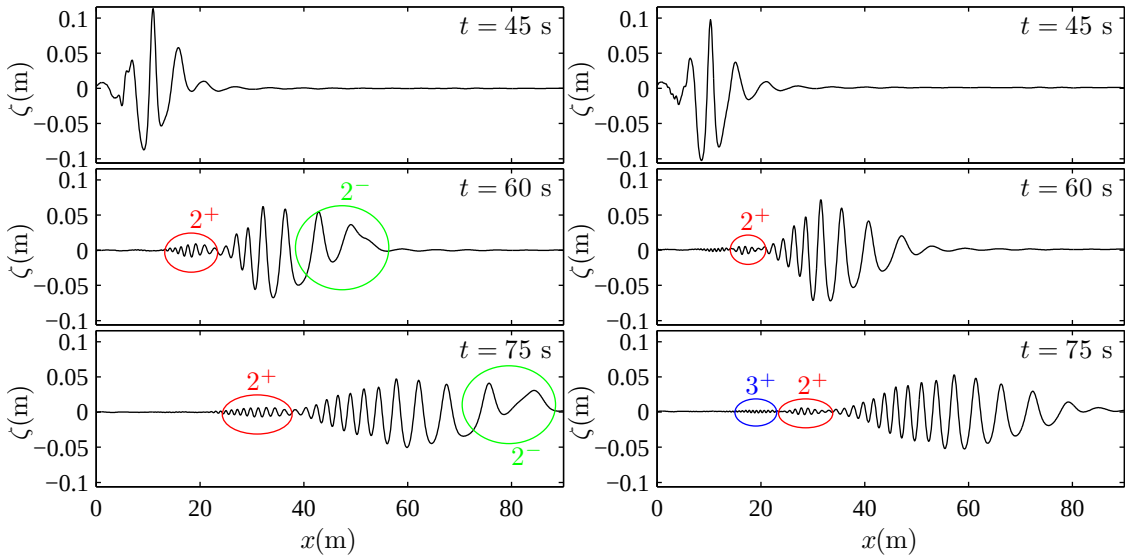


Figure 8: NewWave propagation on a flat bed - spatial profiles for the WG2 crest-focused wave group. Model predictions using a **first-order** paddle signal (left plot) and a **second-order** paddle signal (right plot).

## 4. NewWave run-up at a plane beach

Focused wave group run-up on a plane beach is now investigated. First, the numerical model is validated against laboratory measurements from the UKCRF, using the actual first-order paddle signals as input data. The effect of linear wave generation is then examined numerically by repeating the simulations with second-order accurate paddle signals.

Figure 9 shows the basin setup for the UKCRF run-up experiments, where the basin had the following bed topography: 8.33 m horizontal bed from the paddle followed by a 1:20 plane beach, which extended to well above the still water level. Still water depth at the paddles was 0.5 m. 44 wave gauges, measuring free surface elevation, were deployed at 0.25 m intervals starting at a distance of 6.83 m from the paddles (which is 1.5 m offshore of the beach toe; and where the still water depth was 0.5 m) and finishing at a distance of 17.58 m (which is 0.75 m offshore of the still water line; and where the still water depth was 0.0375 m).

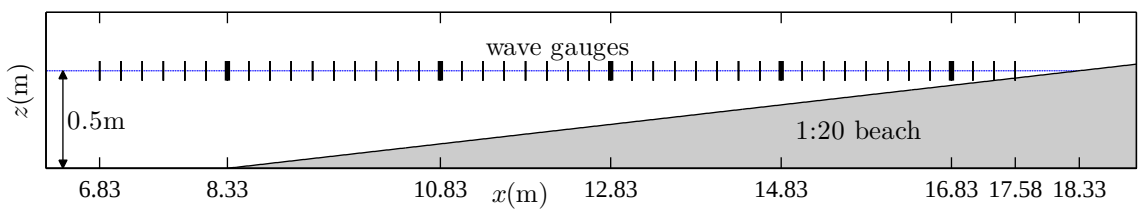


Figure 9: Basin setup and wave gauge placement for the UKCRF run-up experiments. Note that the gauge locations shown in bold are used in Figures 14 and 18.

### 4.1. Model validation

Converged, stable results were obtained for grid resolution $\Delta x = 2$ cm and time step $\Delta t = 0.007$ s, with recorded first-order paddle displacement signals used to drive the numerical paddle. Figures 10 to 13 present the numerical (left plot) and experimental results (right plot) for wave groups WG2 and WG6. Each figure comprises an $x - t$ contour plot determined from the 44 stacked free surface time series (corresponding to the locations of the wave gauges), where the colour represents the free surface deviation from still water depth.

Figure 10 shows the $x - t$ propagation of the WG2 crest-focused group. Initially, the group is rather compact, with three main crests (shown in red, orange and yellow) and two troughs (shown in blue). As it propagates up the beach, the group disperses and becomes less well defined. High-frequency waves can be seen trailing the main group. Shoaling is also evident, for example by considering the first crest at $x = 14$ m to $x = 17$ m. Wave breaking can also be deduced, for example from the sudden loss of amplitude of the central crest (around $x = 14.5 - 15$ m in the numerical plot, or around $x = 14$ m in the experimental plot). Long waves can be seen, reverberating along the length of the flume/basin. The numerical model appears to capture all the main features of this propagating and evolving wave group.

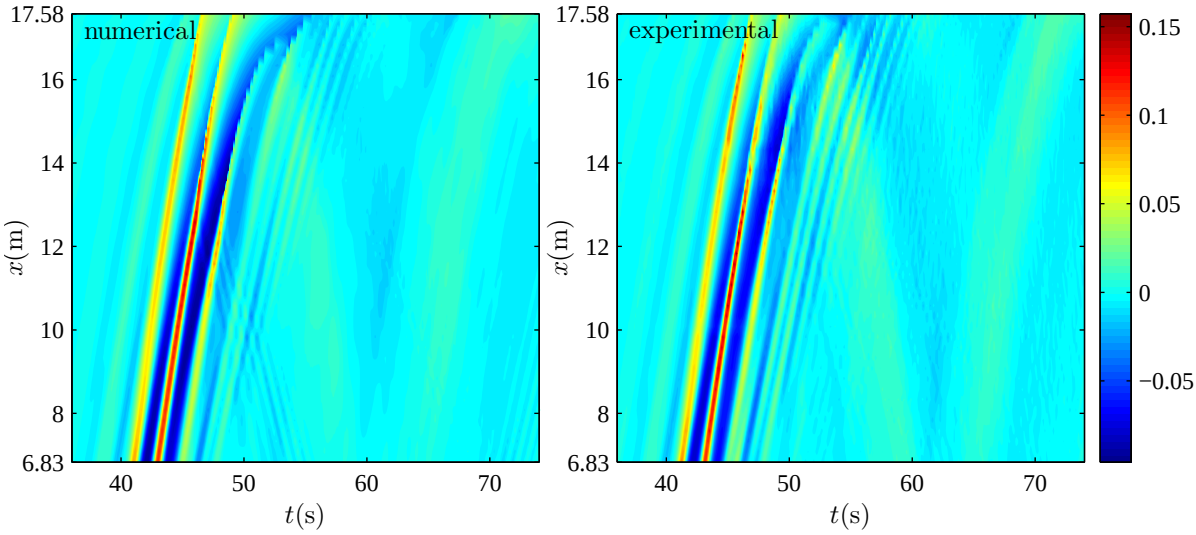


Figure 10: NewWave run-up on a plane beach - **total free surface** for the WG2 crest-focused wave group. Model predictions shown in the left plot. UKCRF measurements shown in the right plot.

Addition, subtraction and filtering are used again to isolate different frequency components. Strictly speaking, these manipulations are not well defined inshore beyond wave breaking or in very shallow water due to mis-alignment of crests and troughs, arising from shallow water non-linear wave-wave interactions of the triad type. However, such analysis can still be useful and is therefore performed at all 44 gauge locations. Figure 11 shows the free surface subtraction time series, low-pass filtered at 1 Hz to isolate the linear terms.

Group dispersion can be seen. There are no visible reflected waves, suggesting that the linear components are dissipated on the beach.

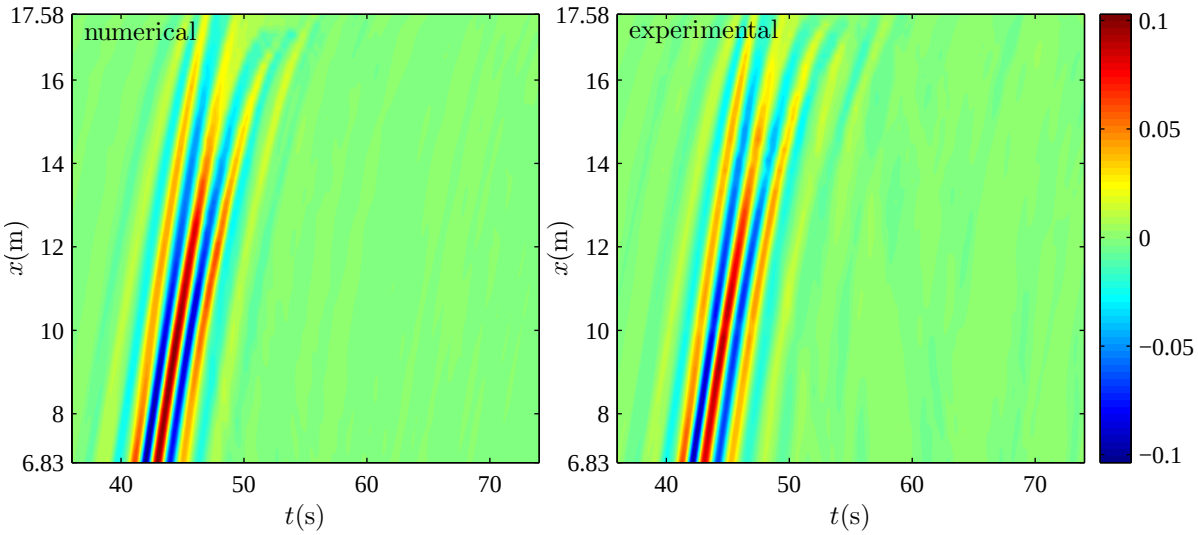


Figure 11: NewWave run-up on a plane beach - **linear terms** only. Model predictions shown in the left plot. UKCRF measurements shown in the right plot.

Figure 12 shows the free surface addition time series, low-pass filtered at 0.5 Hz. The second-order long error wave can be seen as a positive elevation (shown in yellow, orange and red) propagating ahead of and underneath the front of the main wave packet. The second-order bound waves, the set-down underneath the group, can be seen as a depression (shown in blue). The initially bound long waves and the free long error waves are not dissipated at the beach and can be seen sloshing in the flume/basin throughout the entire record, with the bound waves being released at the beach and then propagating as free components. The agreement between the model output and the experimental measurements is generally good.

Figure 13 shows the free surface addition time series, high-pass filtered at 0.5 Hz. These high frequency waves, predominantly second-order sum components, are dissipated at the beach as there are no significant reflected waves coming back from the beach to the paddles. Both the bound and the free error sum frequency harmonics are present in the numerical results and the experiments. The free error waves (denoted by e) can be seen following the bound waves (denoted by b) as they propagate more slowly than the main group.

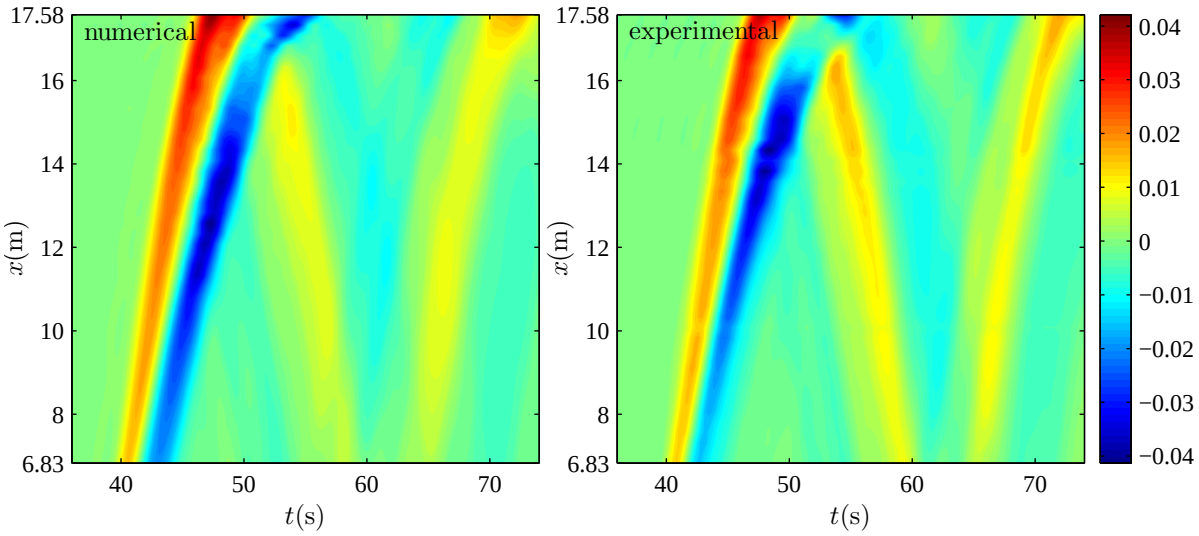


Figure 12: NewWave run-up on a plane beach - **long waves** only. Model predictions shown in the left plot. UKCRF measurements shown in the right plot.

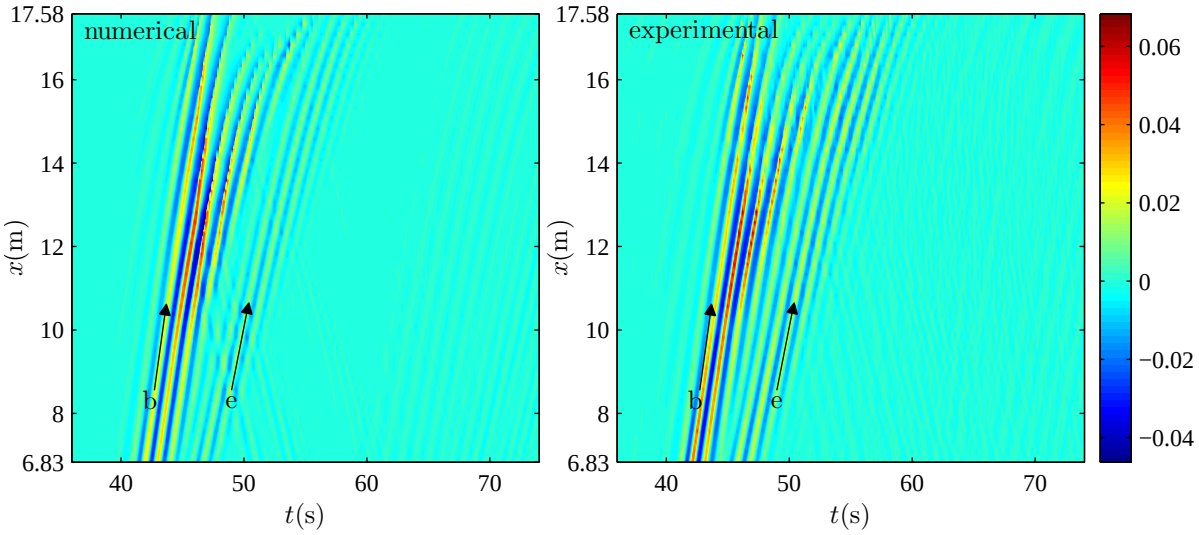


Figure 13: NewWave run-up on a plane beach - **Even-order super-harmonics** only. Model predictions shown in the left plot. UKCRF measurements shown in the right plot.

Figure 14 shows the predicted and measured free surface time series at five locations (highlighted with bold lines in Figure 9). In the crest-focused case, there is a mismatch between the predicted and measured values of the central crest height and the second trough depth at the first two locations. Wave breaking and bore formation appear to be well captured by the model, apart from a slight time shift in some of the broken waves. Turning to the trough-focused case, there is a mismatch in the predicted and measured values of the first crest height and the central trough depth at the first location. Overall, although

there are small differences, it is clear that the numerical model reproduces adequately the evolution of both the crest-focused and trough-focused wave groups as they propagate up the beach.

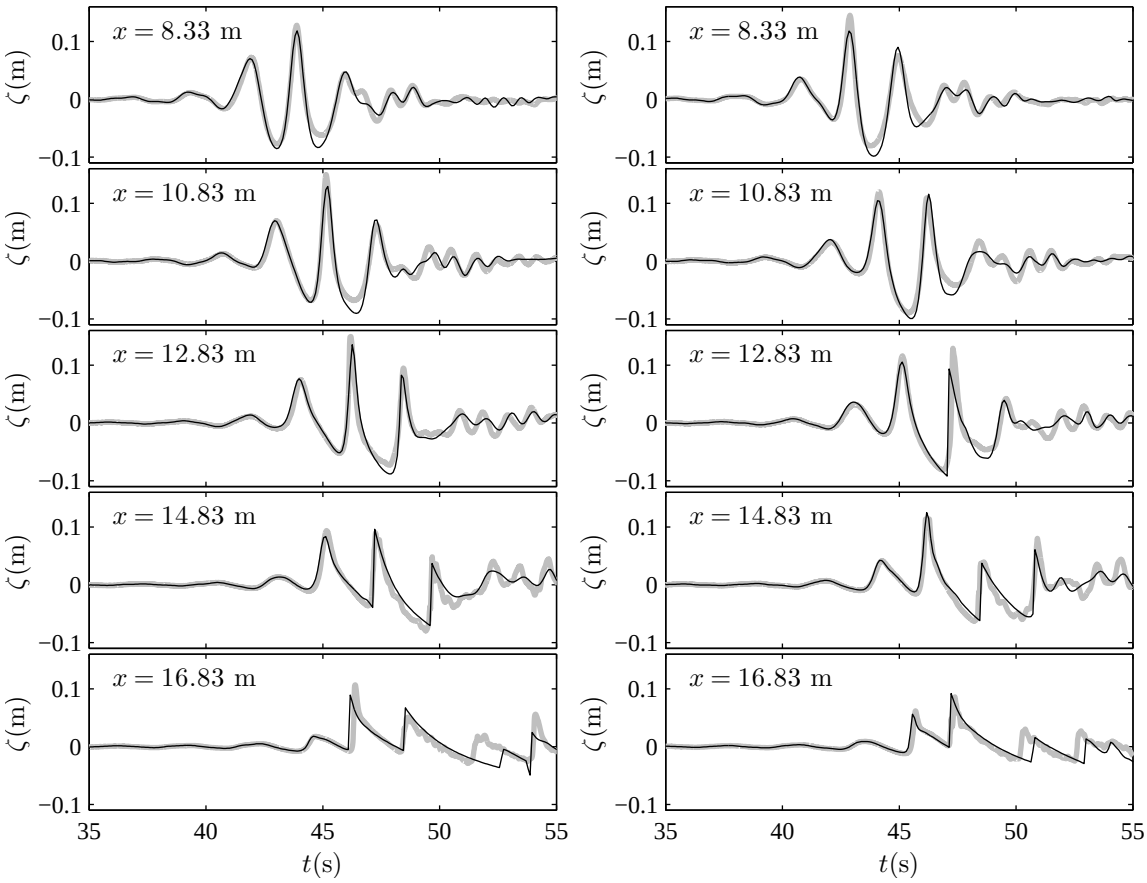


Figure 14: NewWave run-up on a plane beach - free surface time series for the WG2 crest-focused wave (left) and the WG6 trough-focused wave (right). Model predictions shown in thin black line. UKCRF measurements shown in thick grey line.

Figure 15 and Table 2 show the good agreement achieved between the measured and predicted values of horizontal run-up obtained for the eight NewWave cases considered, although it should be noted that the predicted run-up values are all slightly larger than those measured. The maximum error in the model run-up prediction is about 15 %, whereas the average error (of the eight simulations) is about 6 %. The inferred experimental error in the measured run-up values is about 5 % (see Hunt-Raby et al. (2011)). In general, run-up increases with linear amplitude of the wave group, with crest-focused wave groups producing smaller values of run-up compared to their trough-focused counterparts. The numerical model mirrors this behaviour.

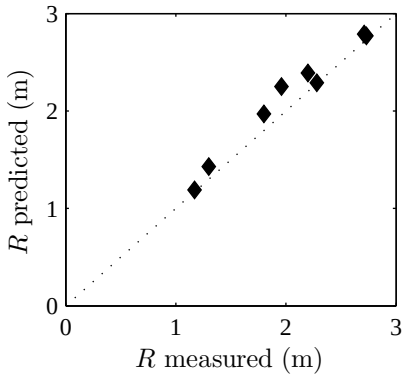


Figure 15: Horizontal run-up of NewWave. Comparison between the model predictions and the UKCRF measurements.

Table 2: Horizontal run-up of NewWave. Comparison between the model predictions and the UKCRF measurements.

| Wave group | Horizontal $R$ measured (m) | Horizontal $R$ predicted (m) | % error |
|---|---|---|---|
| WG1 | 1.96 | 2.25 | 14.8 |
| WG2 | 2.20 | 2.39 | 8.6 |
| WG3 | 1.80 | 1.97 | 9.4 |
| WG4 | 1.17 | 1.19 | 1.7 |
| WG5 | 2.71 | 2.79 | 3.0 |
| WG6 | 2.73 | 2.77 | 1.5 |
| WG7 | 2.28 | 2.29 | 0.4 |
| WG8 | 1.30 | 1.43 | 10.0 |

### *4.2. Effect of long error wave on NewWave run-up*

The influence of the error waves, induced by first-order wave generation, on the run-up of NewWave focused wave groups is now investigated numerically. The error waves comprise a low-frequency hump travelling ahead of the main group and high-frequency waves trailing the main group. As shown in Section 3, the long error wave can be almost completely eliminated by the use of a second-order paddle displacement signal calculated according to Schäffer (1996). The second-order sum frequency error waves can only be partially weakened, but as they travel behind the main wave packet, they will not affect the maximum run-up. The eight run-up simulations involving NewWave groups are reproduced numerically again, this time using paddle signals correct to second order.

Figures 16 and 17 present a comparison between using a first- (left plot) and a second-order paddle signal (right plot) for wave groups WG2 and WG6. Each figure comprises an $x-t$ contour plot of the numerically calculated free surface deviation from still water depth. The figures are centred on the propagating wave group to investigate the effect of the error waves on the resulting wave form, which ultimately influences the run-up distance.

The difference between using a first- and a second-order paddle signal is evident in Figure 16 which shows the $x - t$ propagation of the WG2 crest-focused group. In the first-order case, the left crest is much more pronounced throughout the entire record and breaks further inshore. The central crest, similarly, is higher in the first-order case, and propagates further up the beach. The right crest and the high frequency waves trailing the main group do not appear to be significantly affected by the use of the second-order paddle signal.

Figure 17 shows the extracted long wave components. Use of the second-order paddle signal has a profound effect on the long waves. The free wave, previously traveling ahead of the group, is eliminated when second-order signal is used. The bound long wave can now be clearly seen as a depression underneath the main wave packet. The pronounced left crests and flatter left troughs observed in the first-order cases in Figure 16 are due to this spurious long wave hump.

The free surface time series from five locations along the beach, presented in Figure 14, are revisited in Figure 18 with the wave groups created using a second-order paddle signal superimposed in red. At $x = 8.33$ m and 10.83 m, the WG2 crest-focused wave group (shown on the left) created using the second-order wave-maker has a smaller left crest and deeper left and right troughs. Also, the second-order generated crests lag slightly behind the corresponding first-order generated crests which experience contamination from the long error wave, an advection effect as the wiggles ride on the long error wave. As the WG2 group propagates further up the beach, the left crest is consistently smaller and the central crest breaks earlier. For this reason, in the second-order case, the waves reaching the top of the beach are considerably smaller. This leads to the significantly reduced run-up values listed in Table 3. The WG6 trough-focused wave group (shown on the right) generated with a second-order paddle signal also exhibits deeper troughs and delayed crests. The left crest, which in the first-order case leads to the maximum run-up, is smaller throughout the propagation process, resulting in a much shorter run-up distance.

Figure 19 and Table 3 indicate that the predicted maximum horizontal run-up values obtained using second-order paddle displacement signals are on average about 40 % lower than those obtained using first-order signals. This is a significant difference, indicating that it is undesirable to use linear paddle signals to generate transient focused wave groups for wave run-up estimates.

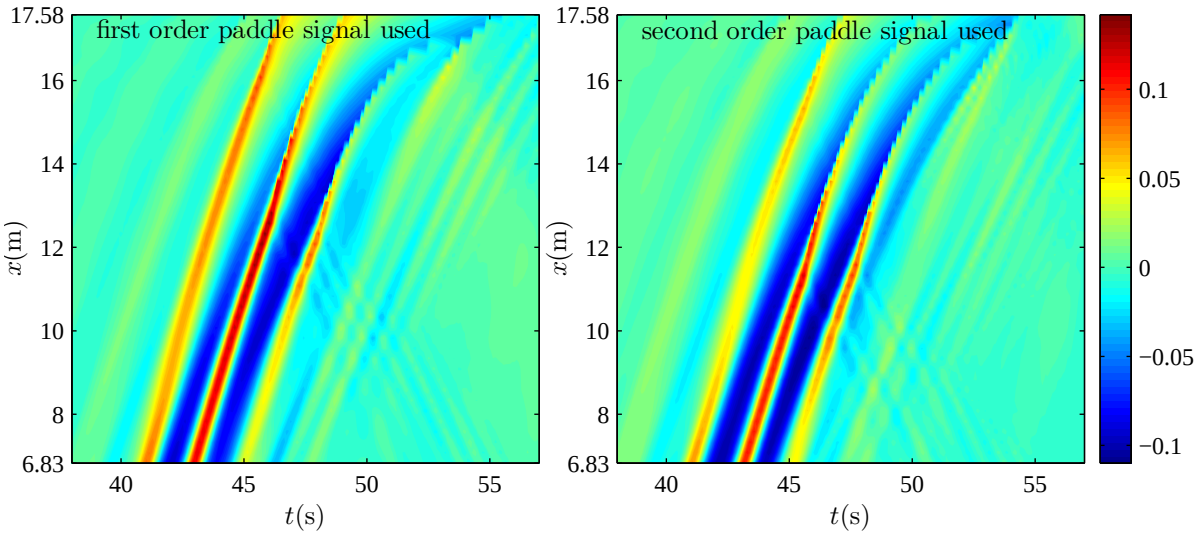


Figure 16: NewWave run-up on a plane beach - **total free surface** for the WG2 crest-focused wave group. Model predictions using a first-order paddle signal (left plot) and a second-order paddle signal (right plot).

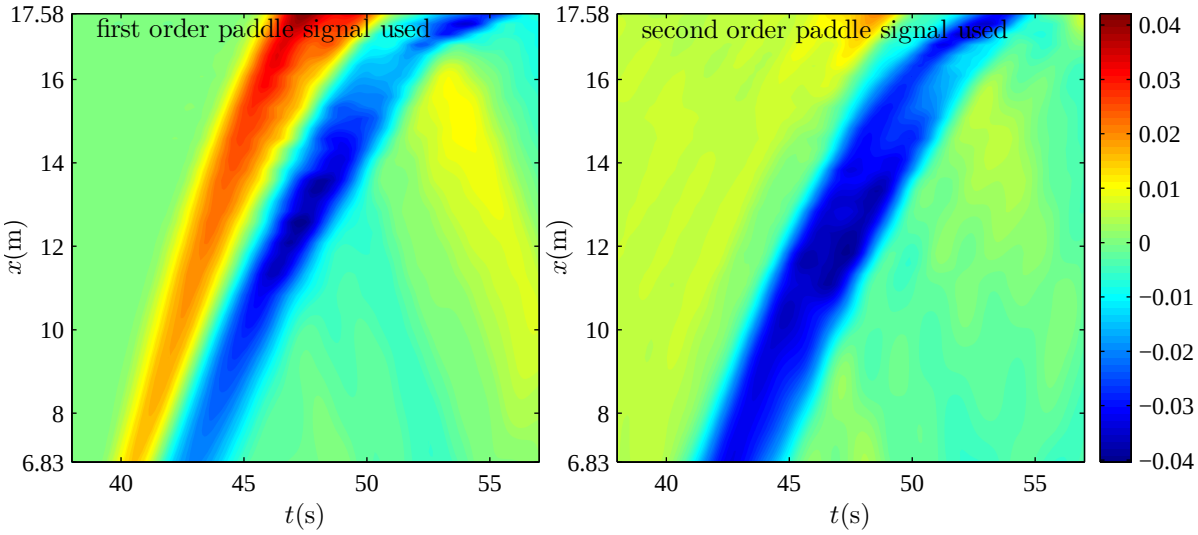


Figure 17: NewWave run-up on a plane beach - **long waves** only. Model predictions using a first-order paddle signal (left plot) and a second-order paddle signal (right plot).

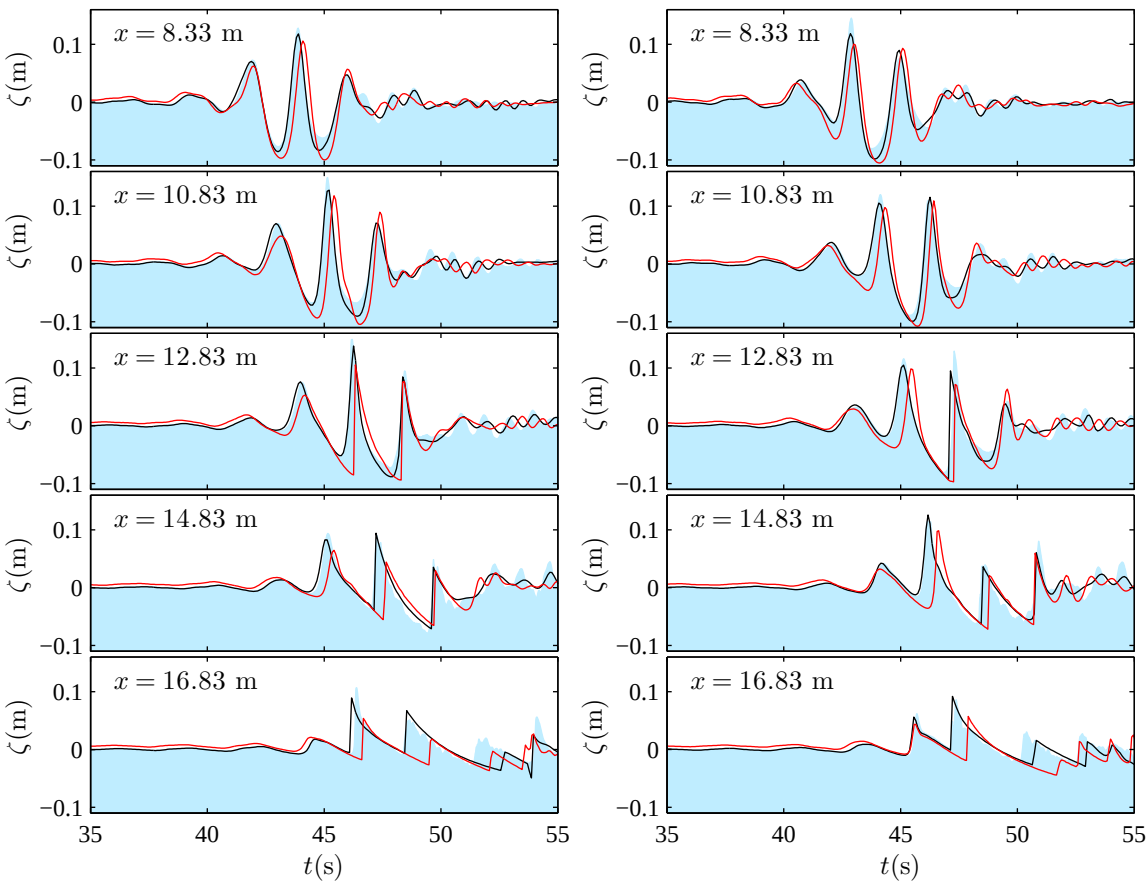


Figure 18: NewWave run-up on a plane beach - free surface time series for the WG2 crest-focused wave (left) and the WG6 trough-focused wave (right). Model predictions when using a first-order paddle signal (black line) and a second-order paddle signal (red line). For reference, UKCRF measurements, using first-order paddle signals, plotted as blue area.

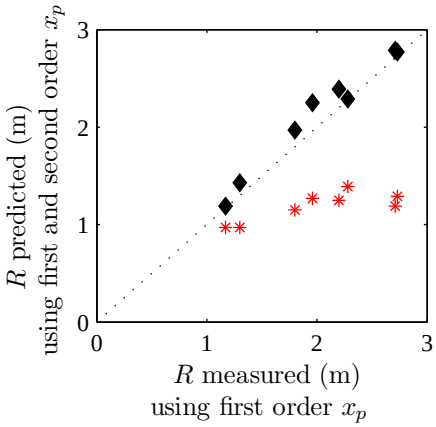


Figure 19: Horizontal run-up of NewWave. Comparison between using first-order (black diamond markers) and second-order (red star markers) paddle displacement signals.

Table 3: Horizontal run-up of NewWave. Comparison between using first- and second-order paddle displacement signals.

| Wave group | Horizontal $R$ (m) using 1st order $x_p$ measured, predicted | | Horizontal $R$ (m) using 2nd order $x_p$ predicted | predicted % difference between using 1st and 2nd order $x_p$ |
|---|---|---|---|---|
| WG1 | 1.96, | 2.25 | 1.27 | -43.6 |
| WG2 | 2.20, | 2.39 | 1.25 | -47.7 |
| WG3 | 1.80, | 1.97 | 1.15 | -41.6 |
| WG4 | 1.17, | 1.19 | 0.97 | -18.5 |
| WG5 | 2.71, | 2.79 | 1.19 | -57.3 |
| WG6 | 2.73, | 2.77 | 1.29 | -53.4 |
| WG7 | 2.28, | 2.29 | 1.39 | -39.3 |
| WG8 | 1.30, | 1.43 | 0.97 | -32.2 |

## 5. NewWave overtopping a seawall

In order to study wave group-induced overtopping, the focused wave tests listed in Table 1 are repeated for the same offshore bathymetry as for the run-up tests, except for a model seawall mounted on the beach. As for the previous run-up cases in Section 4, the laboratory experiments are reproduced by the numerical model to validate its accuracy in predicting overtopping volumes. The recorded experimental paddle displacement signals, calculated according to linear wave-maker theory, are again used in the numerical reproductions. After validation, the overtopping simulations are repeated with second-order accurate wave generation in order to study the effect of the long error wave on overtopping volumes.

For the UKCRF overtopping experiments, the bathymetry was as follows: 8:33 m of flat bed from the paddles, followed by a 1:20 plane beach with a seawall, such that the offshore toe of the seawall was constructed at a distance of 8.125 m from the beach toe, where the still water depth was approximately 9.4 cm. Wave gauges were placed along the centre line of the basin at 0.5 m intervals in the deeper sections of the beach and at smaller intervals directly in front of and across the seawall. The gauges on the seawall were sunk in small PVC tubes set into the seawall to allow recording of the overtopping flow. Figure 20 shows the basin setup with the gauge layout (top) and details of the seawall dimensions (bottom).

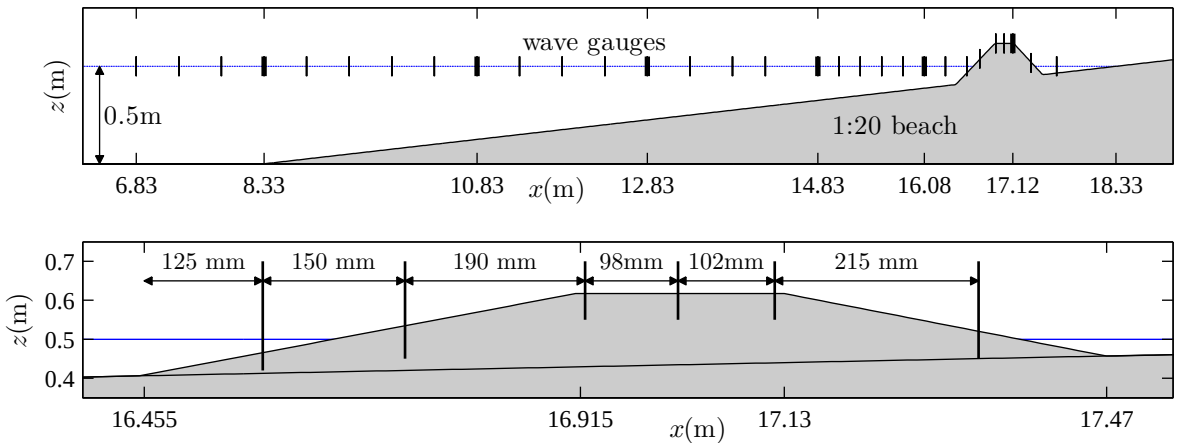


Figure 20: Top plot: basin setup and wave gauge placement for the UKCRF overtopping experiments. Note that the gauge locations shown in bold are used in Figures 21 and 24. Bottom plot: detailed sketch of the seawall and the sunken wave gauges for the UKCRF overtopping experiments.

### *5.1. Model validation*

The Boussinesq numerical model is used to simulate the UKCRF overtopping experiments, with grid resolution $\Delta x = 2$ cm and time step $\Delta t = 0.007$ s, as used for the run-up investigations. A numerical filter is applied in the model to treat potential instabilities arising from sharp reflected waves (off the seawall) re-entering the finite-difference Boussinesq part of the computational domain. First-order paddle displacement signals recorded directly from the laboratory experiments are again used to drive the numerical paddle.

Figure 21 provides a comparison between the numerical and experimental free surface time series at six locations (highlighted with bold lines in Figure 20), starting at the beach toe ($x = 8.33$ m) and finishing at the seawall crest ($x = 17.12$ m). The initial stages of group propagation appear to be well captured by the model. Agreement during the breaking process is not particularly good, but the broken waves are modelled relatively well. Water elevation on the seawall crest associated with overtopping flow is captured in the bottom plots. The initial overtopping (resulting from the central crest for the WG4 crest-focused wave group; and from the left crest for the WG8 trough-focused wave group) is satisfactorily predicted. However, any subsequent overtopping is much less accurately forecast by the model. Note that the model prediction of overtopping volume (per unit length of the seawall) is the worst for the pair WG4 and WG8, as can be seen in Table 4. The maximum error in overtopping volume prediction is about 43 % (noting that this is for small values of overtopping volume), whereas the average error (for the eight simulations) is about 14 %. Values in Table 4 represent the overall overtopped volumes (per unit length of the seawall) after 90 s, and therefore in some cases contain additional overtopping from re-reflected waves. It should also be noted that the inferred experimental error in the measured values of overtopping volume is about 5 %, as calculated from repeat measurements of volumes in the experimental programme.

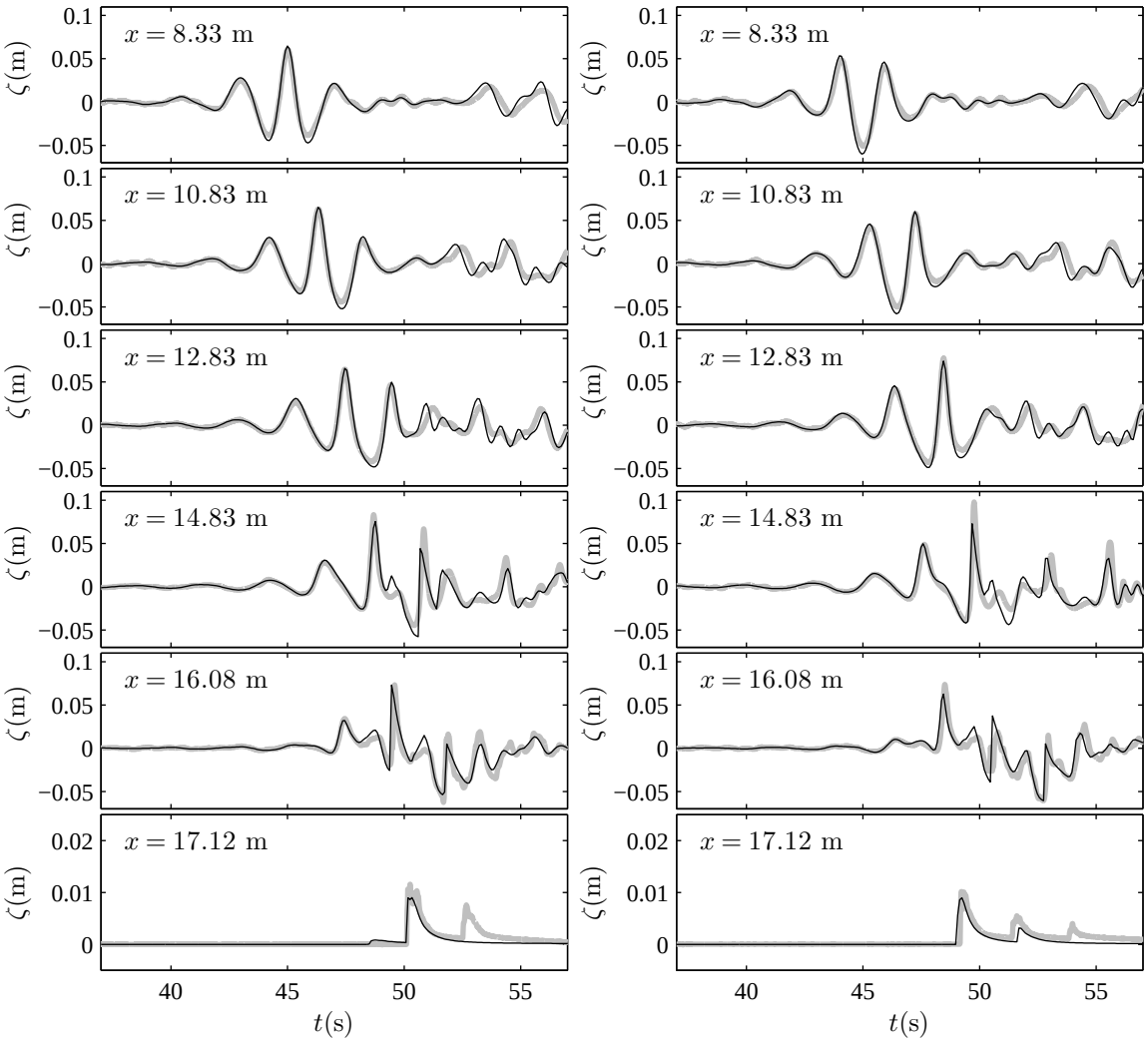


Figure 21: NewWave overtopping a seawall - free surface time series for the WG4 crest-focused wave (left) and the WG8 trough-focused wave (right). Model predictions shown in thin black line. UKCRF measurements shown in thick grey line. Note the vertical scale in the bottom plot (top of the seawall) is magnified.

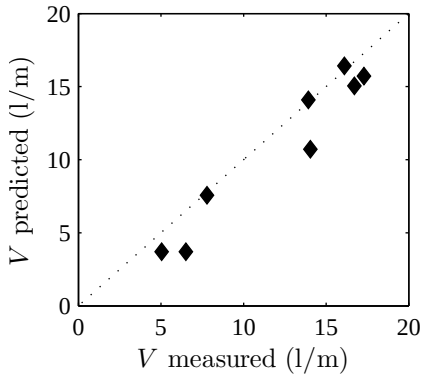


Figure 22: NewWave overtopping volume per unit length of the seawall. Comparison between the model predictions and the UKCRF measurements.

Table 4: NewWave overtopping volume per unit length of the seawall. Comparison between the model predictions and the UKCRF measurements.

| Wave group | $V$ measured (l/m) | $V$ predicted (l/m) | % error |
|---|---|---|---|
| WG1 | 16.10 | 16.41 | 1.9 |
| WG2 | 13.92 | 14.10 | 1.3 |
| WG3 | 7.78 | 7.57 | -2.7 |
| WG4 | 6.51 | 3.71 | -43.0 |
| WG5 | 16.71 | 15.05 | -9.9 |
| WG6 | 17.29 | 15.71 | -9.1 |
| WG7 | 14.05 | 10.71 | -23.7 |
| WG8 | 5.04 | 3.70 | -26.6 |

Figure 23 displays the water surface elevation time series at the seawall crest associated with the overtopping flow for all the NewWave tests, and allows visual comparison of wave-by-wave overtopping events. In all cases, the model captures the main features of the overtopping flow, but at times fails to predict some of the smaller successive overtopping events. As shown in Table 4 and Figure 22, the large volume overtopping cases are well predicted numerically, with the biggest percentage errors occurring for the smaller overtopping groups.

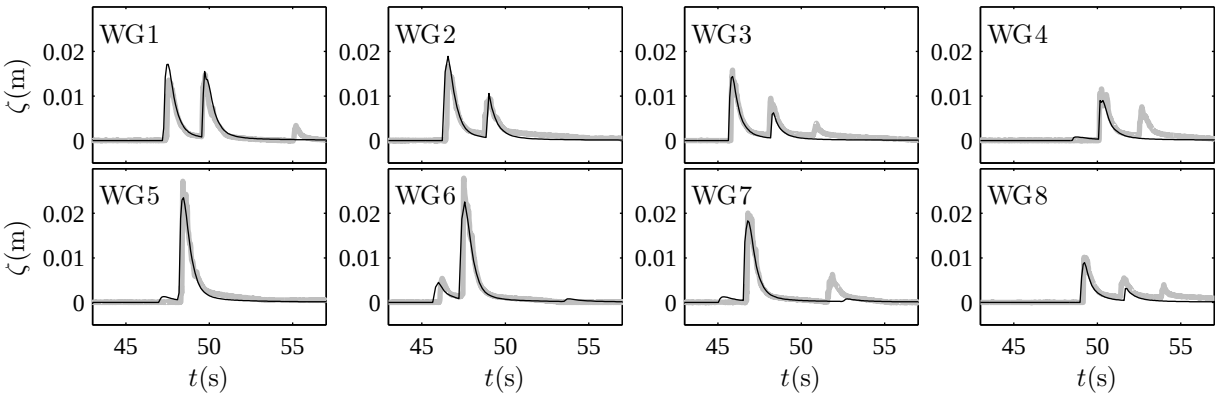


Figure 23: NewWave overtopping a seawall - time variation of the water elevation on the seawall crest ($x = 17.12$ m) associated with the overtopping flow for all eight NewWave groups. Model predictions shown in thin black line. UKCRF measurements shown in thick grey line.

### *5.2. Effect of long error wave on overtopping*

To investigate the effect of the wave-maker second-order error waves on focused wave group overtopping volumes, the eight NewWave overtopping simulations are repeated with second-order paddle displacement signals.

Figure 24 presents a direct comparison between using first- and second-order paddle signals. Free surface time series of the WG1 crest-focused wave group are shown on the left, and of the WG5 trough-focused group on the right. For each wave group, numerical results when using a second-order paddle signal, and numerical and experimental results when using a first-order paddle signal are plotted. When using a second-order signal, the crest-focused wave group has deeper troughs. The left crest is smaller at all locations depicted. The central crest is narrower, lags behind, and breaks earlier the the first-order case. At $x = 16.08$ m, which is 0.375 m offshore of the seawall, the waves are significantly lower in the second-order case, ultimately leading to a limited overtopping flow over the seawall (see the bottom plot at $x = 17.12$ m which is on the seawall crest). The trough-focused wave group generated with a second-order paddle signal also exhibits delayed crests and deeper troughs. The left crest is thinner (meaning it contains less volume) and breaks considerably earlier. Unsurprisingly, it results in a much lower overtopping surge over the seawall. For both wave groups, the underlying long error wave, when using linear wave generation, greatly deforms the wave groups and leads to much larger overtopping.

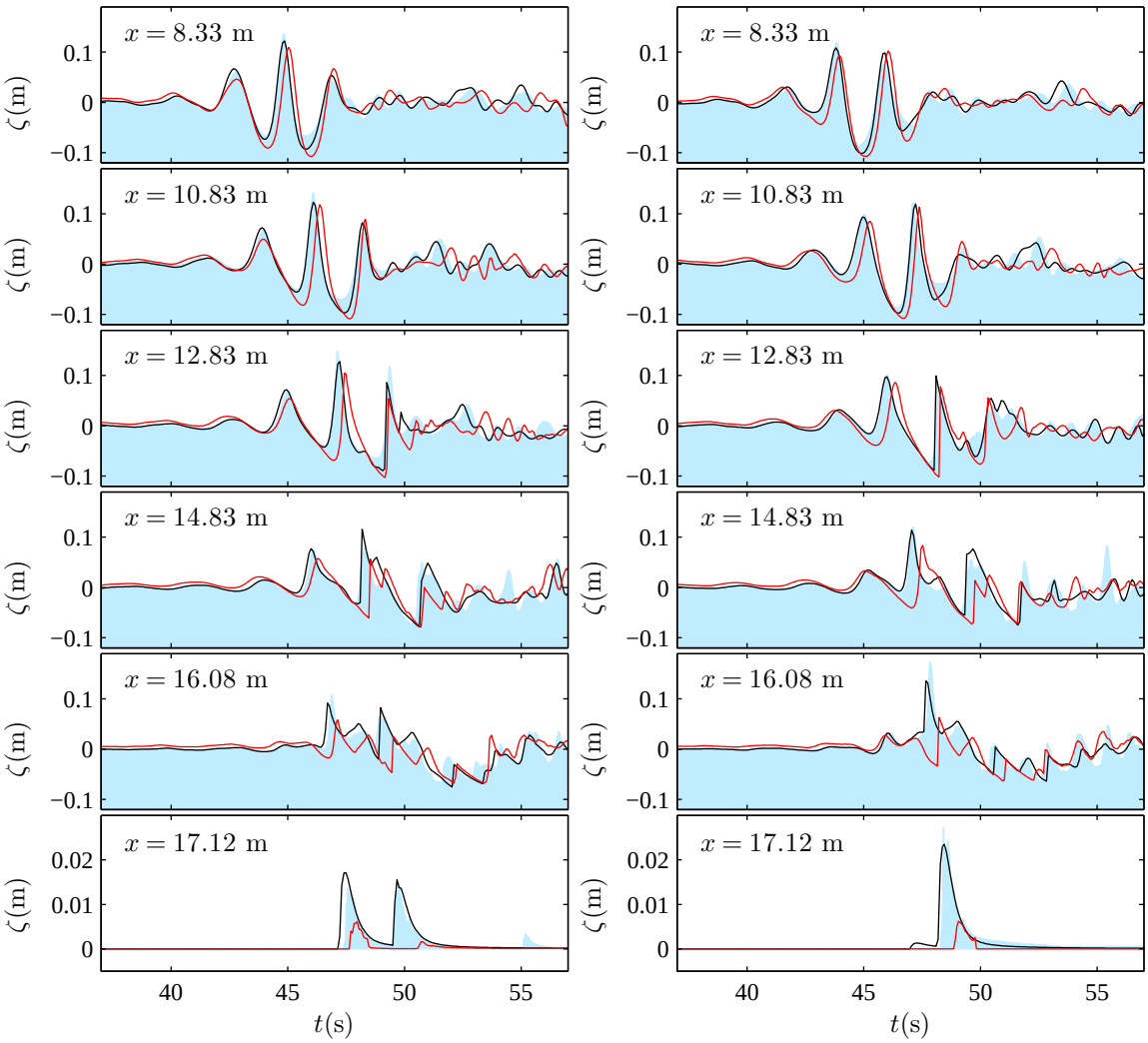


Figure 24: NewWave overtopping a seawall - free surface time series for the WG1 crest-focused wave (left) and the WG5 trough-focused wave (right). Model predictions when using a first-order paddle signal (black line) and a second-order paddle signal (red line). For reference, UKCRF measurements, using first-order paddle signals, plotted as blue area.

Figure 25 displays the wave-by-wave overtopping flow at the seawall crest for all eight NewWave tests. For each wave group, the numerical results obtained using a second-order paddle signal, and numerical and experimental results obtained using a first-order paddle signal are plotted. The overtopping flow is substantially smaller for the second-order paddle signals, which eliminate the long error wave.

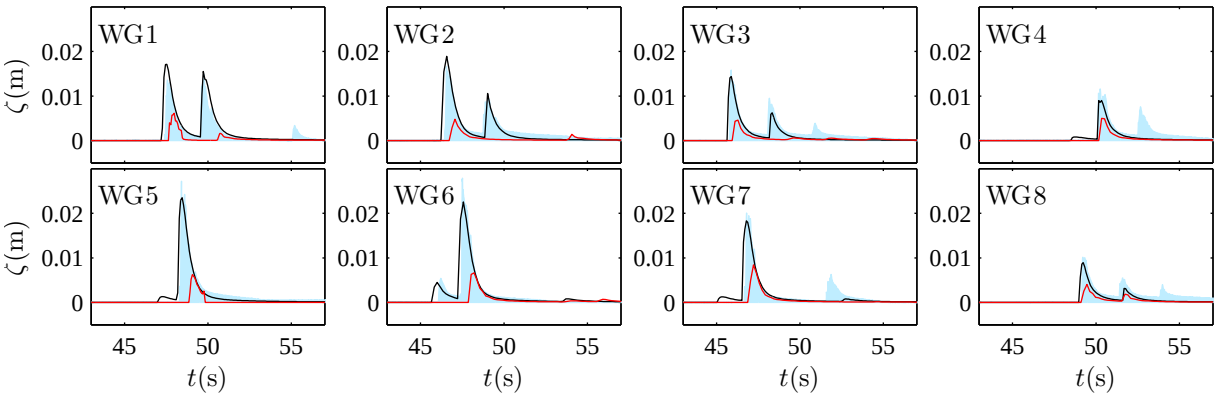


Figure 25: NewWave overtopping a seawall - time variation of the water elevation on the seawall crest ($x = 17.12$ m) associated with the overtopping flow for all eight NewWave groups. Model predictions when using a first-order paddle signal (black line) and a second-order paddle signal (red line). For reference, UKCRF measurements, using first-order paddle signals, plotted as blue area.

Table 5 summarises the overtopping volume per unit length of the seawall for the eight NewWave focused wave groups. The predicted volumes resulting from using second-order paddle displacement signals are compared to the predicted volumes obtained using first-order paddle signals. Recall that this comparison is between nominally the same wave groups, bar the contaminating second-order error waves. The volumes from simulations with the corrected paddle signals are on average around 60% smaller. This is a very large difference; much larger than the model inaccuracies (see Section 5.1 on model validation) or variation in nominally repeated experiments. Figure 26 shows that the resulting overtopping volumes are greatly reduced, and there is much less variation amongst the eight wave groups, when second-order paddle signals are used.

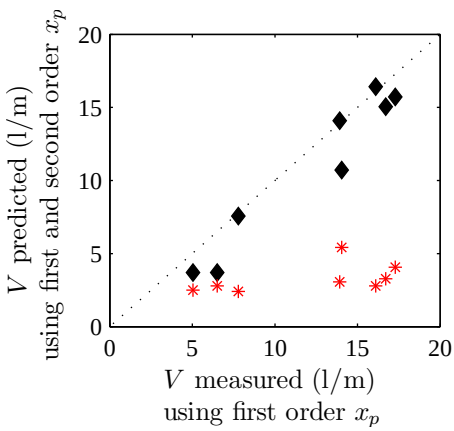


Figure 26: NewWave overtopping volume per unit length of the seawall. Comparison between using first-order (black diamond markers) and second-order (red star markers) paddle displacement signals.

Table 5: NewWave overtopping volume per unit length of the seawall. Comparison between using first- and second-order paddle displacement signals.

| Wave group | Overtopping $V$ (l/m) using 1st order $x_p$ measured, predicted | | Overtopping $V$ (l/m) using 2nd order $x_p$ predicted | predicted % difference between using 1st and 2nd order $x_p$ |
|---|---|---|---|---|
| WG1 | 16.10, | 16.41 | 2.79 | -83.0 |
| WG2 | 13.92, | 14.10 | 3.07 | -78.2 |
| WG3 | 7.78, | 7.57 | 2.41 | -68.1 |
| WG4 | 6.51, | 3.71 | 2.79 | -24.8 |
| WG5 | 16.71, | 15.05 | 3.28 | -78.2 |
| WG6 | 17.29, | 15.71 | 4.07 | -74.1 |
| WG7 | 14.05, | 10.71 | 5.43 | -49.3 |
| WG8 | 5.04, | 3.70 | 2.51 | -32.2 |

## 6. Summary and conclusions

Numerical predictions and laboratory measurements have been presented for NewWave focused wave group run-up at a plane beach and overtopping of a seawall. The numerical model was based on an enhanced version of the Boussinesq equations derived by Madsen and Sørensen (1992) and a balanced form of the non-linear shallow water equations solved using a shock-capturing scheme. The numerical wave tank featured an in-built moving piston wave-maker, which was governed by paddle signals either taken directly from laboratory experiments or calculated according to an appropriate wave-maker theory.

Simulations were made of the evolution of transient wave groups based on NewWave theory propagating over a flat bed. The wave groups were generated according to linear and Schäffer (1996) second-order wave-maker theory. It was found that use of first-order theory gave rise to a significant sub-harmonic error wave that travelled at the front of the group, substantially contaminating the shape of the transient group as it evolved.

The numerical wave tank has been validated extensively against laboratory data obtained from focused wave group run-up and overtopping tests conducted in the U.K. Coastal Research Facility. Close agreement was achieved between predicted and measured propagating wave group profiles, free surface elevation time series, maximum run-up values, and overtopping volumes obtained using the same paddle displacement signals (based on first-order wave-maker theory). By repeating the numerical simulations using a second-order accurate paddle generator, it was possible to assess the likely effect of the error waves induced by the previous first-order wave-maker. Corresponding crest-focused and trough-focused cases were considered in order to interpret the underlying wave groups harmonics. It was found that the long error wave due to linear wave-maker theory spuriously enhanced the wave heights of the leading crests and flattened the troughs. This led to delayed breaking and increased substantially the maximum run-up distances and overtopping volumes. Use of second-order wave generation reduced the predicted maximum horizontal run-up distances by between 18 and 57% and the overtopping volumes by between 25 and 83% over the range

of cases considered. It is therefore concluded that linear wave generation is inadequate for wave group run-up and overtopping studies.

## Acknowledgments

The research was conducted at the Department of Engineering Science, University of Oxford while Jana Orszaghova was a DPhil student under the supervision of Prof. Paul H. Taylor and Prof. Alistair G.L. Borthwick. The work was concluded with Dr Orszaghova working at HR Wallingford, UK, with assistance from Dr James Clarke. The authors would like to thank Prof. Peter K. Stansby and Dr Tong Feng of the University of Manchester, UK for their participation in the UKCRF tests. The U.K. Coastal Research Facility (UKCRF) was co-owned by HR Wallingford and the U.K. Engineering and Physical Sciences Research Council. The laboratory tests were supported by EPSRC Grants GR/R05369, GR/N21741, and GR/N22595. The first- and third-named authors would also like to acknowledge support from EPSRC Grant EP/F020511 as part of the U.K. Flood Risk Management Research Consortium (FRMRC-II).

Agnon, Y., Madsen, P. A., Schäffer, H. A., 1999. A new approach to high-order Boussinesq models. Journal of Fluid Mechanics 399, 319 – 333.

Allsop, W., Bruce, T., Pearson, J., Beasley, P., 2005. Wave overtopping at vertical and steep seawalls. Proceedings of the ICE - Maritime Engineering 158, 103–114.

Baldock, T., 2006. Long wave generation by the shoaling and breaking of transient wave groups on a beach. Proceedings of the Royal Society A: Mathematical, Physical and Engineering Science 462 (2070), 1853–1876.

Baldock, T. E., Peiris, D., Jogg, A. J., 2012. Overtopping of solitary waves and solitary bores on a plane beach. Proceedings of the Royal Society of London. Series A: Mathematical, Physical and Engineering Sciences 468, 3494 – 3516.

Baldock, T. E., Swan, C., Taylor, P. H., 1996. A laboratory study of nonlinear surface waves on water. Philosophical Transactions of the Royal Society of London. Series A: Mathematical, Physical and Engineering Sciences 354 (1707), 649 – 676.

Barthel, V., Mansard, E. P. D., Sand, S. E., Vis, F. C., 1983. Group bounded long waves in physical models. Ocean Engineering 10 (4), 261 – 294.

Boccotti, P., 1983. Some new results on statistical properties of wind waves. Applied Ocean Research 5 (3), 134 – 140.

Borthwick, A. G. L., 2009. Coastal risk: advance or retreat. In: Huang, C., Wiener, J. B., Ni, J. (Eds.), New Perspectives on Risk Analysis and Crisis Response: Proceedings of the 2nd International Conference on Risk Analysis and Crisis Response. Atlantis Press, pp. 15–26.

Borthwick, A. G. L., Ford, M., Weston, B. P., Taylor, P. H., Stansby, P. K., 2006a. Solitary wave transformation, breaking and run-up at a beach. Proceedings of the Institution of Civil Engineers - Maritime Engineering 159, 97 – 105.

Borthwick, A. G. L., Hunt, A. C., Feng, T., Taylor, P. H., Stansby, P. K., 2006b. Flow kinematics of focused wave groups on a plane beach in the U.K. Coastal Research Facility. Coastal Engineering 53, 1033 – 1044.

Brocchini, M., 2013. A reasoned overview on boussinesq-type models: the interplay between physics, mathematics and numerics. Proceedings of the Royal Society A: Mathematical, Physical and Engineering Science 469 (2160).

Brufau, P., Vázquez-Cendón, M. E., García-Navarro, P., 2002. A numerical model for the flooding and drying of irregular domains. International Journal for Numerical Methods in Fluids 39, 247 – 275.

Burcharth, H., Hughes, S., 2006. Fundamentals of design. Engineer Manual 1110-2-1100. U.S. Army Corps of Engineers, Washington, pp. 1 – 23.

De Rouck, J., Geeraerts, J., Troch, P., Kortenhaus, A., Pullen, T., Franco, L., et al., 2005. New results on scale effects for wave overtopping at coastal structures. In: Proceedings of the ICE Conference on Coastlines, Structures and Breakwaters. London, United Kingdom. pp. 29–43.

Dean, R. G., Dalrymple, R. A., 1991. Water Wave Mechanics for Engineers and Scientists. Advanced Series on Ocean Engineering, Volume 2. World Scientific, Singapore.

Dingemans, M. W., 1997. Water Wave Propagation over Uneven Bottoms, Part 2- Non-linear Wave Propagation. Advanced Series on Ocean Engineering, Volume 13. World Scientific, River Edge, NJ.

Fructus, D., Grue, J., 2007. An explicit method for the nonlinear interaction between water waves and variable and moving bottom topography. Journal of Computational Physics 222, 720–739.

Fuhrman, D. R., Madsen, P. A., 2008. Simulation of nonlinear wave run-up with a high-order Boussinesq model. Coastal Engineering 55 (2), 139 – 154.

Gobbi, M. F., Kirby, J. T., Wei, G., 2000. A fully nonlinear Boussinesq model for surface waves. Part 2. Extension to O(kh)$^4$. Journal of Fluid Mechanics 405, 181 – 210.

Hedges, T. S., Mase, H., 2004. Modified Hunt's equation incorporating wave setup. Journal of Waterway, Port, Coastal, and Ocean Engineering 130 (3), 109 – 113.

Hedges, T. S., Reis, M. T., 2004. Accounting for random wave run-up in overtopping predictions. Proceedings of the ICE - Maritime Engineering 157, 113–122.

Hsiao, S.-C., Lin, T.-C., 2010. Tsunami-like solitary waves impinging and overtopping an impermeable seawall: Experiment and {RANS} modeling. Coastal Engineering 57 (1), 1 – 18.

Hu, K., Mingham, C. G., Causon, D. M., 2000. Numerical simulation of wave overtopping of coastal structures using the non-linear shallow water equations. Coastal Engineering 41 (4), 433 – 465.

Hubbard, M. E., Dodd, N., 2002. A 2D numerical model of wave run-up and overtopping. Coastal Engineering 47, 1 – 26.

Hughes, S. A., 1993. Physical Models and Laboratory Techniques in Coastal Engineering. Advanced Series on Ocean Engineering, Volume 7. World Scientific, Singapore ; River Edge, NJ.

Hunt, A. C., 2003. Extreme Waves, Overtopping and Flooding at Sea Defences. Ph.D. thesis, University of Oxford, UK.

Hunt, A. C., Taylor, P. H., Borthwick, A. G., Stansby, P. K., Feng, T., 2004. Phase inversion and the identification of harmonic structure in coastal engineering experiments. Proceedings of the International Conference on Coastal Engineering 1 (29), 1047–1059.

Hunt, I. A. J., 1959. Design of seawall and breakwaters. Journal of Waterway, Port, Coastal, and Ocean Engineering 85 (3), 123 – 152.

Hunt-Raby, A. C., Borthwick, A. G., Stansby, P. K., Taylor, P. H., 2011. Experimental measurement of focused wave group and solitary wave overtopping. Journal of Hydraulic Research 49 (4), 450–464.

Ingram, D., Gao, F., Causon, D., Mingham, C., Troch, P., 2009. Numerical investigations of wave overtopping at coastal structures. Coastal Engineering 56 (2), 190 – 202, the {CLASH} Project Crest Level Assessment of Coastal Structures by Full-scale Monitoring, Neural Network Prediction and Hazard Analysis on Permissible Wave Overtopping (CLASH).

Johannessen, T., Swan, C., 2001. A laboratory study of the focusing of transient and directionally spread surface water waves. Proceedings of the Royal Society of London. Series A: Mathematical, Physical and Engineering Sciences 457 (2008), 971–1006.

Jonathan, P., Taylor, P. H., 1997. On irregular, nonlinear waves in a spread sea. Journal of Offshore Mechanics and Arctic Engineering 119 (1), 37 – 41.

Kirby, J., 1997. Nonlinear, Dispersive Long Waves in Water of Variable Depth. Advances in fluid mechanics. Computational Mechanics Publications.

Kirby, J. T., 2003. Boussinesq models and applications to nearshore wave propagation, surfzone processes and wave-induced currents. Vol. 67 of Elsevier Oceanography Series. Elsevier Science, pp. 1–41.

Kobayashi, N., 1999. Wave runup and overtopping on beaches and coastal structures. Advances in Coastal and Ocean Engineering 5, 95 – 154.

Lindgren, G., 1970. Some properties of a normal process near a local maximum. The Annals of Mathematical Statistics 41, 1870 – 1883.

Madsen, P. A., Bingham, H. B., Schäffer, H. A., 2003. Boussinesq-type formulations for fully nonlinear and extremely dispersive water waves: derivation and analysis. Proceedings of the Royal Society of London. Series A: Mathematical, Physical and Engineering Sciences 459, 1075 – 1104.

Madsen, P. A., Schäffer, H. A., 1999. A review of Boussinesq-type equations for surface gravity waves. Advances in Coastal and Ocean Engineering 5, 1 – 94.

Madsen, P. A., Sørensen, O. R., 1992. A new form of the Boussinesq equations with improved linear dispersion characteristics. Part 2. A slowly-varying bathymetry. Coastal Engineering 18, 183 – 204.

Madsen, P. A., Sørensen, O. R., 1993. Bound waves and triad interactions in shallow water. Ocean Engineering 20 (4), 359 – 388.

McCabe, M., Stansby, P., Apsley, D., 2013. Random wave runup and overtopping a steep sea wall: Shallow-water and boussinesq modelling with generalised breaking and wall impact algorithms validated against laboratory and field measurements. Coastal Engineering 74 (0), 33 – 49.

Orszaghova, J., Borthwick, A. G., Taylor, P. H., 2012. From the paddle to the beach - A Boussinesq shallow water numerical wave tank based on Madsen and Sørensen's equations. Journal of Computational Physics 231 (2), 328 – 344.

Pearson, J., Bruce, T., Allsop, N., Gironella, V., 2002. Violent wave overtopping - measurements at large and small scale. p. 12.

Pullen, T., Allsop, W., Bruce, T., Kortenhaus, A., Schuettrumpf, H., van der Meer, J., 2007. EurOtop - Wave Overtopping of Sea Defences and Related Structures: Assessment Manual. http://www.overtopping-manual.com/eurotop.pdf.

Rapp, R. J., Melville, W. K., 1990. Laboratory measurements of deep-water breaking waves. Philosophical Transactions of the Royal Society of London. Series A, Mathematical and Physical Sciences 331 (1622), 735–800.

Rogers, B. D., Dalrymple, R. A., 2008. SPH modeling of tsunami waves. Advances in coastal and ocean engineering. World Scientific, Ch. 3, pp. 75–100.

Schäffer, H. A., 1996. Second-order wavemaker theory for irregular waves. Ocean Engineering 23 (1), 47 – 88.

Taylor, P. H., Williams, B. A., 2004. Wave statistics for intermediate depth water - NewWaves and symmetry. Journal of Offshore Mechanics and Arctic Engineering 126 (1), 54 – 59.

Tissier, M., Bonneton, P., Marche, F., Chazel, F., Lannes, D., 2011. Serre green-nanghdi modelling of wave transformation breaking and run-up using a high-order finite-volume finite-difference scheme. Proceedings of the International Conference on Coastal Engineering 1 (32).
URL `https://journals.tdl.org/ICCE/article/view/1235`

Tonelli, M., Petti, M., 2009. Hybrid finite volume - finite difference scheme for 2DH improved Boussinesq equations. Coastal Engineering 56, 609 – 620.

Tromans, P. S., Anaturk, A. R., Hagemeijer, P., 1991. A new model for the kinematics of large ocean waves application as a design wave. In: Proceedings of the First International Offshore and Polar Engineering Conference. Vol. 3. pp. 64 – 71.

Tucker, M. J., Pitt, E. G., 2001. Waves in ocean engineering. Elsevier Ocean Engineering Book Series, Volume 5. Elsevier, Amsterdam; New York.

van der Meer, J. W., Verhaeghe, H., Steendam, G. J., 2009. The new wave overtopping database for coastal structures. Coastal Engineering 56 (2), 108 – 120, the CLASH Project - Crest Level Assessment of Coastal Structures by Full-scale Monitoring, Neural Network Prediction and Hazard Analysis on Permissible Wave Overtopping (CLASH).

Watson, G., Barnes, T., Peregrine, D., 1994. The generation of low-frequency waves by a single wave group incident on a beach. Coastal Engineering Proceedings 1 (24).

Wei, G., Kirby, J. T., Grill, S. T., 1995. A fully nonlinear Boussinesq model for surface waves. I. Highly nonlinear unsteady waves. Journal of Fluid Mechanics 294, 71 – 92.

**LaTeX Source Files**

**Click here to download LaTeX Source Files: Coastal_Eng_paper_2014_2nd_submission_after_reviewers_comments.zip**